

Department of Physics, Chemistry and Biology

Master's Thesis

Search for Dark Matter in the Upgraded High Luminosity LHC at CERN

Impact of ATLAS phase II performance on a mono-jet analysis

Sven-Patrik Hallsjö

Thesis work performed at Stockholm University

Linköping, June 4, 2014

LITH-IFM-A-EX--14/2863--SE



**Linköpings universitet
TEKNISKA HÖGSKOLAN**

Department of Physics, Chemistry and Biology
Linköping University
SE-581 83 Linköping, Sweden

Search for Dark Matter in the Upgraded High Luminosity LHC at CERN

Impact of ATLAS phase II performance on a mono-jet analysis

Sven-Patrik Hallsjö

Thesis work performed at Stockholm University

Linköping, June 4, 2014

Supervisor: **Docent Christophe Clément**
 FYSIKUM Stockholm University
Professor Magnus Johansson
 IFM, Linköping University

Examiner: **Professor Magnus Johansson**
 IFM, Linköping University



Avdelning, Institution
Division, Department

Theoretical physics group
Department of Physics, Chemistry and Biology
SE-581 83 Linköping

Datum
Date

2014-06-04

Språk
Language

Svenska/Swedish
 Engelska/English

Rapporttyp
Report category

Licentiatavhandling
 Examensarbete
 C-uppsats
 D-uppsats
 Övrig rapport

ISBN
—

ISRN
LITH-IFM-A-EX--14/2863--SE

Serietitel och serienummer **ISSN**
Title of series, numbering —

URL för elektronisk version

<http://urn.kb.se/resolve?urn=urn:nbn:se:liu:diva-XXXXXX>

Titel Sökandet efter mörk materia i den uppgraderade hög luminositets LHC i CERN
Title Search for Dark Matter in the Upgraded High Luminosity LHC at CERN

Undertitel Påverkan av ATLAS fas II prestanda på en mono-jet analys
Subtitle Impact of ATLAS phase II performance on a mono-jet analysis

Författare Sven-Patrik Hallsjö
Author

Sammanfattning
Abstract

Disclaimer: Abstract not yet completed.

Something as an introduction:

The LHC at CERN is undergoing an upgrade to increase the center of mass energy for the colliding particles which means that new physical processes will be explored. One drawback of this is that it will be harder to isolate unique particle collisions since more and more collisions will occur simultaneously, so called pile-up.

One hope for the upgrade is that WIMP models of dark matter will be detected.

This thesis covers looking at effective operators which try to explain dark matter without adding new theories to the standard model or QFT.

Some results and a slight conclusion.

Nyckelord

Keywords

Disclaimer: This not yet completed., ATLAS, Beyond standard model physics, CERN, Dark matter, Elementary particle physics, High energy physics, something, this is in mythesis.sty

4 **Abstract**

5 **Disclaimer: Abstract not yet completed.**

6 Something as an introduction:

7 The LHC at CERN is undergoing an upgrade to increase the center of mass en-
8 ergy for the colliding particles which means that new physical processes will be
9 explored. One drawback of this is that it will be harder to isolate unique parti-
10 cle collisions since more and more collisions will occur simultaneously, so called
11 pile-up.

12 One hope for the upgrade is that WIMP models of dark matter will be detected.

13 This thesis covers looking at effective operators which try to explain dark matter
14 without adding new theories to the standard model or QFT.

15 Some results and a slight conclusion.

16 **Acknowledgments**

17 [REDACTED]

18 A big thank you to my family, fiancée and friends who have supported me through-
19 out my education. A warm thank you to my friend Joakim Skoog who altered
20 some of the images for me.

21 [REDACTED]

22 [REDACTED]

23 *Linköping, June 2014*
24 *Sven-Patrik Hallsjö*

Contents

Notation

1 Introduction

1.1	Research goals	2
1.2	Theoretical Background	3
1.2.1	Quantum mechanics and quantum field theory	3
1.2.2	Nuclear, particle and subatomic particle physics	4
1.2.3	The standard model of particle physics	4
1.2.4	Dark matter	5
1.2.5	Effective field theory	6
1.2.6	Search for WIMPS	8
1.3	Experimental overview	10
1.3.1	LHC	10
1.3.2	ATLAS	11
1.3.3	Coordinate system	12
1.3.4	Reconstructing data	12
1.3.5	Pile-up	13
1.3.6	Mono-jet analysis	13
1.3.7	Phase II high luminosity upgrade	14
1.3.8	Monte Carlo simulation	15

2 Validation of smearing functions

2.1	Smearing functions	18
2.1.1	Electron and photon	18
2.1.2	Muon	18
2.1.3	Tau	18
2.1.4	Jets	18
2.1.5	Missing Transversal Energy	18
2.2	Validation	20
2.3	Results	21
2.3.1	Electron and photon	22
2.3.2	Muon	23
2.3.3	Tau	23

58	2.3.4 Jets	24
59	2.3.5 Missing Transversal Energy	25
60	2.4 Expected results	26
61	2.5 Discussion	28
62	2.5.1 Smearing independent on pile-up	28
63	2.5.2 Comparison to expected results	28
64	2.6 Conclusion	29
65	3 Evaluating dark matter signals	31
66	3.1 Signal to background ratio	32
67	3.1.1 Selection criteria	32
68	3.1.2 Verifying background data	32
69	3.1.3 Weight	33
70	3.1.4 Figure of merit	33
71	3.1.5 D5 operators	34
72	3.1.6 Light vector mediator models	34
73	3.2 Other selection criteria	35
74	3.2.1 Criteria	35
75	3.2.2 Verifying background data	35
76	3.3 Mitigating the effect of the high luminosity	36
77	3.4 Results	37
78	3.4.1 Verifying background data	37
79	3.4.2 Events	37
80	3.4.3 Limit on M^*	38
81	3.4.4 Effect of pile-up on M^*	41
82	3.4.5 Previous results	41
83	3.4.6 Limit on mediator mass	41
84	3.4.7 Effect of pile-up on mediator mass	42
85	3.5 Discussion	43
86	3.5.1 Comparison to previous results	43
87	3.5.2 Effect of the high luminosity	43
88	3.6 Conclusion	44
89	3.6.1 Limit on M^*	44
90	3.6.2 Limit on mediator mass	44
91	4 Results and Conclusions	45
92	4.1 Validation of smearing functions	45
93	4.2 Signal to background ratio	46
94	4.2.1 Limit on M^*	46
95	4.2.2 Limit on mediator mass	46
96	4.3 Other selection criteria and observables	46
97	4.3.1 Limit on M^*	46
98	4.3.2 Limit on mediator mass	46
99	4.4 Mitigating the effect of the high luminosity	46
100	4.5 Recommendations to mitigate the effect of the high luminosity	46
101	4.6 Suggestions for future research	46

102	A Datasets	49
103	A.1 Background processes	49
104	A.1.1 Validation	49
105	A.1.2 Background to signals	49
106	A.2 Signals	50
107	A.2.1 Qcut	50
108	A.2.2 D5 signal processes	50
109	A.2.3 Light vector mediator processes	50
110	Bibliography	55

Notation

NOTATIONS

Notation	Explanation
barn(b)	$1 \text{ barn}(b) = 10^{-24} \text{ cm}^2$
\oplus	$a \oplus b = \sqrt{a^2 + b^2}$, $a \oplus b \oplus c = \sqrt{a^2 + b^2 + c^2}$

ABBREVIATIONS

Abbreviation	Expansion
ATLAS	A large Toroidal LHC ApparatuS
CERN	Organisation européenne pour la recherche nucléaire ¹
CMS	Compact Muon Solenoid
CR	Control Region
LHC	Large Hadron Collider
MC	Monte Carlo
RMS	Root Mean Square
SM	the Standard Model of particle physics
SR	Signal Region
WIMP	Weakly Interacting Massive Particle
WIMPS	Weakly Interacting Massive ParticleS
QED	Quantum ElectroDynamics
QFT	Quantum Field Theory
QM	Quantum Mechanics

¹Originally, Conseil Européen pour la Recherche Nucléaire

1

Introduction

117 Discrepancies in measurements of the rotations of galaxies indicate the presence
118 of a large amount of matter which interacts through gravity, though not elec-
119 tromagnetically making it invisible to our telescopes. This matter is commonly
120 referred to as dark matter. Since no known or hypothesised particle in the stan-
121 dard model of particle physics can be used as a candidate for dark matter, this
122 hints at the presence of new physics.

123 At the Organisation Européene pour la Recherche Nucléaire (CERN) focus now
124 lies to discover any evidence of so called weakly interacting massive particles
125 (WIMPS) which may be a candidate for dark matter. It is usually impossible to
126 detect any interaction of dark matter candidates on the subatomic scale, however
127 through looking at proposed interactions, searching for assumed decay channels
128 and by investigating what is invisible to the detectors by using momentum con-
129 servation it is hoped that signs will be found. Though to date, none have been
130 found.

131 Both experiments and current theories now show that higher energies are re-
132 quired at the LHC to be able to see any signs. This is why the LHC and all detectors
133 are undergoing a vast upgrade program [1]. In this thesis focus will be on the last
134 part of the upgrade due for completion in 2023, known as the high luminosity-
135 LHC phase II upgrade; and also on the ATLAS detector. The method used in this
136 thesis focuses on looking at data which emulate conditions at the upgraded LHC.

137 1.1 Research goals

138 This research took place at Stockholm University from January 7th until **when**?
139 During the research period the following tasks were set up and performed/answered:

- 140 • Implement a C++ programme that loops over the collisions inside the signal
141 and background datasets.
- 142 • For each collision retrieve the relevant observables (variables used to extract
143 the signal over the background) and apply "smearing functions" to emulate
144 the effect of the high luminosity on the observables.
- 145 • For both signal and background datasets, compare observables before and
146 after smearing. What observables are the least/most affected?
- 147 • Implement selection criteria that selects the signal collisions efficiently while
148 reduces significantly the background. In a first step the selection criteria
149 should be taken from existing studies.
- 150 • Selection criteria can be evaluated and compared with each other using a
151 figure of merit P , that measures the sensitivity of the experiment to the dark
152 matter signal. Calculate P for the given selection criteria before and after
153 smearing.
- 154 • What is the effect of the high luminosity (smearing) on the value of P ?
- 155 • Investigate other selection criteria and observables, to mitigate the effect of
156 high luminosity. Use P to rank different criteria after smearing.
- 157 • Conclude on the effect of the high luminosity on the sensitivity for dark matter
158 and possible ways to mitigate its effects using alternative observables
159 and selection criteria.

1.2 Theoretical Background

1.2.1 Quantum mechanics and quantum field theory

In the beginning of the 20th century, some physical phenomena could not be explained by classical physics, for example the ultra-violet disaster of any classical model of black-body radiation, and the photoelectric effect [2]. It was these phenomena that led to the formulation of quantum mechanics (QM), where energy transfer is quantized and particles can act as both waves and particles at the same time [3].

Combining QM with classical electromagnetism proved harder than expected, colliding a photon(em-field) and an electron (particle/wave) is quite tricky. This can be seen when trying to calculate the scattering between them both in a QM schema. One idea that came from this was to explain them both in the same framework, field theory. Also, trying to incorporate special relativity into QM suggested a field description where space-time is described using the metric formalism from differential geometry. The culmination of both of these problems is the first part of a Quantum field theory (QFT), Quantum electrodynamics (QED) which with incredible precision explains electromagnetic phenomena including effects from special relativity[4]. It is in this merging that antimatter was theorised, since it is a requirement for the theory to hold. After the discovery of antimatter, the theory was set in stone. Since this the theory has been altered somewhat to explain more and more experimental data. This is discussed more in subsection 1.2.2 and subsection 1.2.3.

To be able to calculate properties in QFT one uses the Lagrangian formalism [5], which gives a governing equation for the different physical processes. In general the Lagrangian used for the Standard model is quite complicated, one can thus focus on one of the different terms corresponding to a specific interaction. This can be done to calculate the so called cross-section for a process, which is related to the probability that that process will occur. A step to simplify the calculations is to use the so called Feynman diagrams, an example of which is given in figure 1.1.

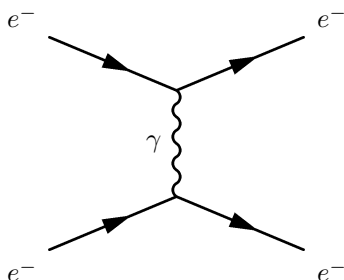


Figure 1.1: An example of a Feynman diagram explaining an electron-electron scattering using QED.

Through the figure, which comes with certain rules, and knowing what the major process (in this case QED) one can calculate the cross-section [4]. It is this that is needed to predict what one will be able to detect new particles.

1.2.2 Nuclear, particle and subatomic particle physics

Many could argue that these branches of physics started after Ernest Rutherford famous gold foil experiment [6], where he discovered that matter is composed of matter with a nucleus, a lot of empty space and electrons.

It was this that sparked the curiosity to see what the nucleus is made of and what forces govern the insides of atoms. After this, and the combination of the theoretical description given by QM, a lot more has been discovered and still more has been predicted. The newest of these is of course the Higgs particle, which was predicted through QFT and then discovered by the ATLAS and the CMS experiments at CERN [7].

The discovered particles are often divided into different groups depending on the fundamental particles that build them up. For instance, particles build up of three quarks are known as hadrons. Particles with an integer spin are known as bosons whereas half-integer particles are known as fermions.

1.2.3 The standard model of particle physics

The standard model of particle physics, referred to simply as the standard model (SM), is the particle zoo which tries to categorize all the particles and that have been discovered experimentally. QFT explains the interactions between these particles and it has also predicted several particles by including symmetries [6]. Regarding SM, Gauge bosons are the force carriers for the different forces, quarks are the and leptons are the fundamental blocks that we know of so far. The difference between the later two is if they interact via the strong force or not.

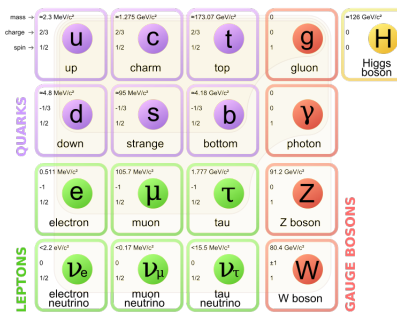


Figure 1.2: The standard model of particle physics where the three first columns represent the so called generations, starting with the first. [8].

SM is today the pinnacle of particle physics and can be used to explain almost everything that occurs around us. There are however some problems [9]:

- There is no link between gravity and the SM.
- Asymmetry between matter and antimatter can not be fully explained.
- No dark matter candidate!
- No explanation that can contain dark matter.

221 In this thesis focus lies with dark matter, some more introduction to possible
 222 dark matter and different candidates in extensions to SM are explained in subsection
 223 1.2.4.

224 1.2.4 Dark matter

225 Dark matter is among other things, the name given to the solution to the discrepancies
 226 of galactic rotations.

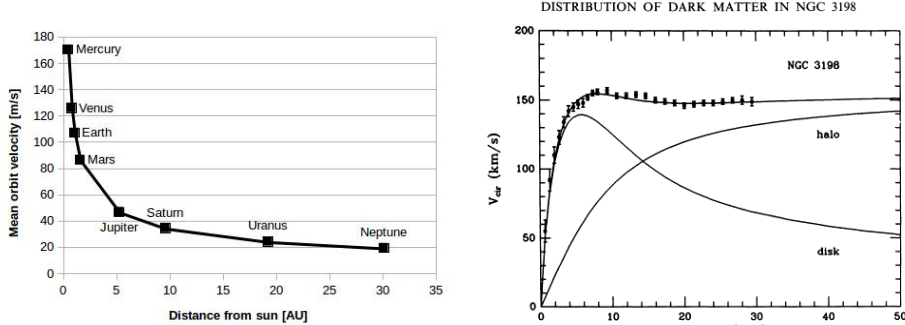
227 To explain this, focus on matter in a galaxy which are rotating around the center
 228 of the galaxy. Through Newtons law of gravity and the centrifugal force one can
 229 calculate the rotation speed dependent on the distance to the center of the galaxy.
 230 Since one of these forces is attractive and the other repulsive, if the matter is in
 231 a stable orbit around the galactic center (which they are) they must be equal and
 232 give us an expression for the speed depending on the distance. Newtons law can
 233 be written as the following:

$$F_{Gravitational} = G \frac{Mm}{r^2} = G_M \frac{m}{r^2} \quad F_{Centrifugal} = m \frac{V^2}{r} \quad (1.1)$$

234 where G is the gravitational constant, M the mass of the centre object, m the mass
 235 of the matter, r the distance between the two and V is the rotation speed. It has
 236 been simplified using G_M since all matter orbits the same galactic center. Setting
 237 the equations in (1.1) results in:

$$G_M \frac{m}{r^2} = m \frac{V^2}{r} \Leftrightarrow V^2 = \frac{G_M}{r} \Rightarrow V = \sqrt{\frac{G_M}{r}} \propto \frac{1}{\sqrt{r}} \quad (1.2)$$

238 where the speed is assumed to be positive and \propto means proportional. Through
 239 these simple calculations it shown that the rotation speed should decrease with
 240 and increased distance. The same reasoning can be applied to our solar system
 241 where this is the case figure 1.3a. The relation in these units is $V = \frac{107}{\sqrt{r}}$ where
 242 107 can be used in (1.2) to calculate the mass of the sun. However when looking
 243 at galaxies, even when taking into account that one has to see the galaxies as a
 244 mass distribution and that the above is only true when outside of the inner mass
 245 half, this is not the case! In figure 1.3b experimental data can be seen from the
 246 galaxy NGC3198 with a fitted curve which does not decrease with the distance
 247 but is instead constant. This is the discrepancy which is solved by postulating
 248 the existence of dark matter. After this the big question arises, what could this
 249 dark matter consist of? What is known so far lies in the name. It is called dark
 250 since there is no electromagnetic interaction and matter since it has gravitational
 251 interaction. This means that it can not be made up of any baryonic matter or
 252 anything in the Standard Model apart from neutrinos. The main interest of this
 253 thesis and also the main contributor to the rotational discrepancies is known as
 254 cold dark matter. This is due to the matter having a low speed, thus low kinetic
 255 energy, and have a high particle mass (In the GeV scale) [9, 12, 13]. This means
 256 however that neutrinos can not be a candidate, thus dark matter can not be made
 257 out of any standard model particles. There are several ideas to detected dark
 258 matter, [9]



(a) *Rotation speed of planets in our solar system. Since the distance is quite small on an astronomical scale, there is no sign of dark matter. Based on data from [10].*

(b) *Rotation speed of matter in NGC3198 with a curve fitting and three different models, if only a dark model halo existed, if there was no dark matter and the correct, if both exist [11].*

Figure 1.3: Different rotation curves, both for planets in our solar system and matter in the NGC3198 galaxy.

- Ordinary matter interacting with ordinary matter can produce dark matter, known as production. Which is the processes that occurs at particle accelerators.
- Dark matter interacting with ordinary matter can produce dark matter, known as direct detection.
- Dark matter interacting with dark matter can produce ordinary matter, known as indirect detection.

In this thesis the focus lies with production. There are several theories how to detect dark matter in proton-proton collisions such that occur at the LHC at CERN this is covered more in subsection 1.2.6.

1.2.5 Effective field theory

In quantum field theory the objective is usually to find the part of the Lagrangian which explains a type of interaction, known as the operator of the interaction and also to find the probability amplitude (cross-section) for a certain interaction. For complicated processes it is easier to employ certain conditions so that the small scale phenomena are simplified and the whole picture understood. This is known as using an effective field theory and the concept is explained in figure 1.4. The operator can be found through assuming the possible interactions and using the effective field theory [4]. The cross-sections can be found through the Feynman diagrams as described in subsection 1.2.1.

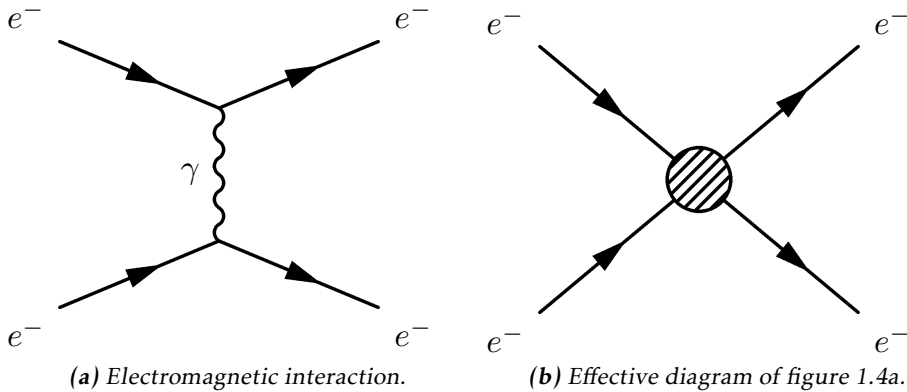


Figure 1.4: Feynman diagram of an electron-electron scattering, both as an ordinary diagram and as its effective theory version, where the details are hidden in the blob.

In this thesis the same effective field theory as in Refs. [12, 14] will be considered. The WIMP (usually denoted χ) is assumed to be the only particle in addition to the standard model fields. It is assumed that an even number of χ must be in every coupling. It is assumed that the mediator exists is heavier than the WIMPS, meaning that their interactions are in higher order terms of the effective field theory and thus not included in the operators. For simplicity, the WIMPS are assumed to be SM singlets, thus invariant under SM gauge transformations, and the coupling to the Higgs boson is neglected.

The operators used in this thesis are assumed to be quark bilinear operators on the form $\bar{q}\Gamma q$ where Γ is a 4×4 matrix of the complete set,

$$\Gamma = \{1, \gamma^5, \gamma^\mu, \gamma^\mu \gamma^5, \sigma^{\mu\nu}\} \quad (1.3)$$

This will dictate how the operators are written, more of why this is done can be found in [4, 12, 14].

This defines an effective field theory of the interaction of singlet WIMPs with hadronic matter. It is an approximation which will break down when the mediator mass is close to the mass of the WIMP. The condition for this is derived in [14] and gives:

$$M > 2m_\chi \quad (1.4)$$

where m_χ is the mass of the WIMP and M is the mass of the mediator particle. There is also the requirement that:

$$M \lesssim 4\pi M_* \quad (1.5)$$

where M_* is the energy scale where the effective theory is no longer a good approximation.

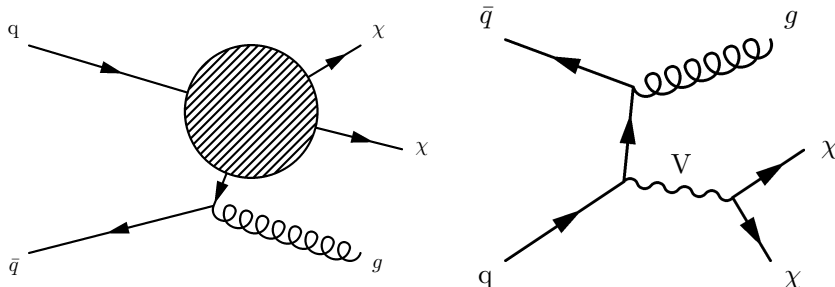
²⁹⁹ In this work, WIMPS are assumed to be Dirac fermions (half integer spin and is
³⁰⁰ not its own antiparticle).

³⁰¹ In table 1.1 the operators which are integrated out via the effective field theory
³⁰² and are of interest in this thesis are given.

Name	Initial state	Type	Operator
D1	qq	scalar	$\frac{m_q}{M_*^3} \bar{\chi} \chi \bar{q} q$
D5	qq	vector	$\frac{1}{M_*^2} \bar{\chi} \gamma^\mu \chi \bar{q} \gamma_\mu q$
D8	qq	axial-vector	$\frac{1}{M_*^2} \bar{\chi} \gamma^\mu \gamma^5 \chi \bar{q} \gamma_\mu \gamma^5 q$
D9	qq	tensor	$\frac{1}{M_*^2} \bar{\chi} \sigma^{\mu\nu} \chi \bar{q} \sigma_{\mu\nu} q$
D11	gg	scalar	$\frac{1}{4M_*^3} \bar{\chi} \chi \alpha_s (G_{\mu\nu}^a)^2$

Table 1.1: Table based on discussion in [13].

³⁰³ Where D denotes that the WIMPS are assumed to be Dirac fermions. These can all
³⁰⁴ be described using figure 1.5a.



(a) Effective Feynman diagram explaining the D-operators. **(b)** Feynman diagram describing the vector mediator model.

Figure 1.5: Feynman diagrams describing the signal models used in this thesis.

³⁰⁵ Another model which is considered is a vector mediator model which is described
³⁰⁶ by figure 1.5b.

1.2.6 Search for WIMPS

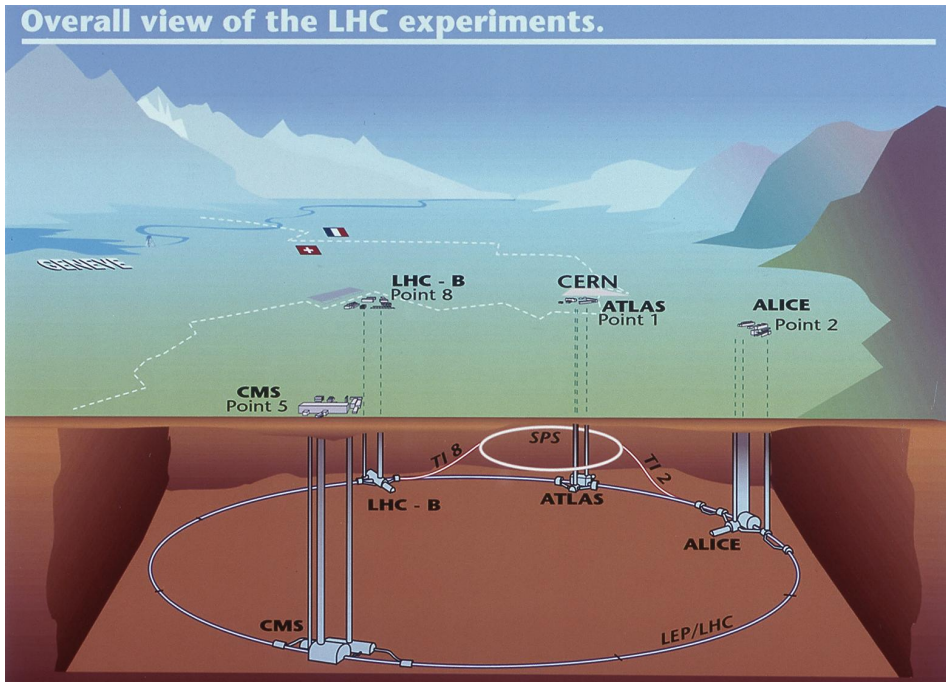
³⁰⁸ The search for WIMPS is based on a mono-jet analysis which is described in sub-
³⁰⁹ section 1.3.6. This method revolves around a high energetic jet which arises from
³¹⁰ the gluon from figure 1.5b and momentum missing from the energy conservation.

- 311 This means that something has happened which the detectors can not detect. If
312 the models from subsection 1.2.5 can explain the missing energy, then a model
313 for WIMPS has been found.
- 314 Since the search for WIMPS at the LHC is based on looking at the missing energy,
315 not actual detection, the experiment can not establish if a WIMP is stable on a
316 cosmological time scale and thus if it is a dark matter candidate [13]. This means
317 that if a candidate is found, it may still not be the dark matter that is needed to
318 explain the cosmological observations.
- 319 The different theories discussed in subsection 1.2.5 require some process in which
320 quarks and anti-quarks are produced. At ATLAS they have looked at proton-
321 proton collisions, in which they are produced, with 8 TeV center of mass energy
322 with out finding any excess of mono-jet events. This is why it is very interesting
323 that the LHC is undergoing a upgrade that will allow higher energy levels, see
324 subsection 1.3.7. With this the processes can be given higher energy and thus the
325 produced particles can be comprised of higher mass.

326 1.3 Experimental overview

327 1.3.1 LHC

328 The large hadron collider (LHC) is a particle accelerator located at CERN near
 329 Geneva in Switzerland, see figure 1.6. The accelerator was built to explore physics
 330 beyond the standard model and to make more accurate measurements of stan-
 331 dard model physics. Before it was shut down for an upgrade in 2012 it was able
 332 to accelerate two proton beams to such a velocity that each proton in them had
 333 an energy of 4 TeV which gives a center of mass energy, $\sqrt{s} = 8$ TeV. The proton
 334 beam is comprised of bunches of protons with enough spacing that bunch col-
 335 lisions can happen independent of each other. Apart from the energy, the rate at
 336 which the accelerator produces a certain process can be calculated through the
 337 instantaneous luminosity. For the LHC the instantaneous luminosity was 10^{34}
 338 $\text{cm}^{-2}\text{s}^{-1}$ [15] or $10\text{nb}^{-1}\text{s}^{-1}$ where 1 barn(b)= 10^{-24} cm^2 .



339 **Figure 1.6:** Figure showing the LHC and the different detector sites[16].

340 The instantaneous luminosity, often just denoted luminosity, can be defined in
 341 different ways depending on how the collision takes place. For two collinear
 intersecting particle beams it is defined as:

$$342 \mathcal{L} = \frac{f k N_1 N_2}{4\pi \sigma_x \sigma_y} \quad (1.6)$$

342 where N_i are the number of protons in each of the bunches, f is the frequency
 343 at which the bunches collide , k the number of colliding bunches in each beam,
 344 and σ_x (σ_y) is the horizontal (vertical) beam size at the interaction point. Since
 345 the instantaneous luminosity increases quadratically with more protons in each
 346 bunch, increasing the number of protons would be a good strategy to increase
 347 the instantaneous luminosity. However aside from the difficulties to create and
 348 maintain a beam with more particles, a large N_i increases the probability for
 349 multiple collisions per bunch crossing, referred to as pile-up. Pile up will be a
 350 key aspect which is described more in subsection 1.3.5.

351 The expected number of events can be calculated by using the instantaneous lu-
 352 minosity through the following:

$$N = \sigma \int \mathcal{L} dt \equiv \sigma \mathcal{L} \quad (1.7)$$

353 where \mathcal{L} is the integrated luminosity and σ is the cross section which is often
 354 measured in barn. The integrated luminosity is a measurement of total number
 355 of interactions that have occurred over time. Before the LHC was shut down \mathcal{L}
 356 was 20.8 fb^{-1} .

357 The cross section, as explained in subsection 1.2.1, is a measure of the effective
 358 surface area seen by the impinging particles, and as such is expressed in units
 359 of area. The cross section is proportional to the probability that an interaction
 360 will occur. It also provides a measure of the strength of the interaction between
 361 the scattered particle and the scattering center. Further details can be found in
 362 reference [17].

363 1.3.2 ATLAS

364 As seen in figure 1.6, there are several detectors at the LHC. One of these is
 365 ATLAS which is a general purpose detector that uses a toroid magnet. Its goal
 366 is to observe several different production and decay channels. The detector is
 367 composed of three concentric sub-detectors, the Inner detector, the Calorimeters
 368 and the Muon spectrometer [18].

369 The Inner detectors main task is to detect the tracks of the particles. It also mea-
 370 sures the position of the initial proton-proton collision.

371 The Calorimeters, electromagnetic and hadronic, are used to calculate the energy
 372 contained in the different particles. The electromagnetic detects particles which
 373 are charged, and the hadronic those which are neutral.

374 The Muon spectrometer is used to detect signs of muons, which will simply pass
 375 through the other detectors without leaving a trace. It also calculates the energy
 376 and momentum of the muons.

377 The neutrinos escape the ATLAS experiment without being detected, and in this
 378 thesis it is assumed that WIMPS pass through all the detectors without leaving
 379 any trace.

380 1.3.3 Coordinate system

381 The coordinate system of ATLAS, seen in figure 1.7 is a right-handed coordinate
 382 system with the x-axis pointing towards the centre of the LHC ring, and the z-axis
 383 along the tunnel/beam (counter clockwise) seen from above. The y-axis points up-
 384 ward. The origin is defined as the geometric center of the detector. A cylindrical
 385 coordinate system is also used for the transversal plane, (R, ϕ, Z) . For simplicity
 386 the pseudorapidity of particles from the primary vertex is defined as:

$$\eta = -\ln(\tan \frac{\theta}{2}) \quad (1.8)$$

387 where θ is the polar angle (xz-plane) of the particle direction measured from
 388 the positive z-axis. η is through this definition invariant under boosts in the z-
 389 direction.

390 It is quite common to calculate the distance between particles and jets in the
 391 (η, ϕ) space, $d = \sqrt{(\Delta\eta)^2 - (\Delta\phi)^2}$.

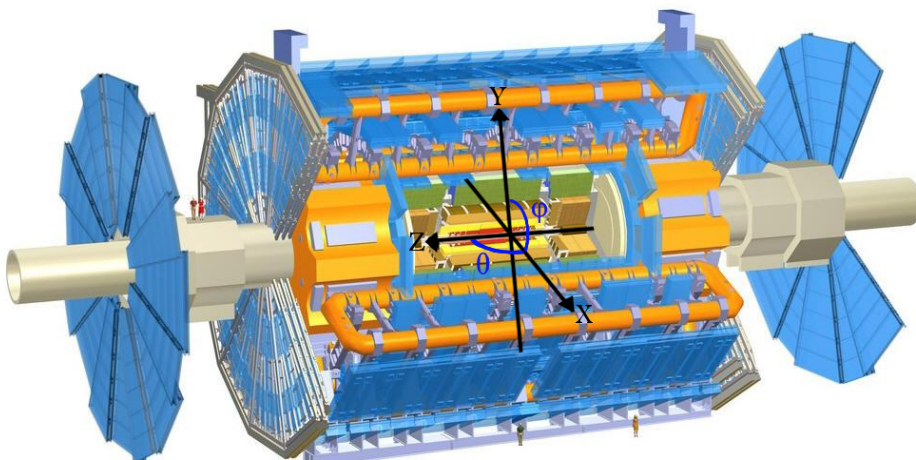


Figure 1.7: The ATLAS detector and the definition of the orthogonal Cartesian coordinate system. Image altered from[19]

392 1.3.4 Reconstructing data

393 To be able to compare the simulated data to real data it is important to include
 394 effects of the detectors. This is done using so called smearing functions which try
 395 to emulate the reconstruction of data.

396 The reconstruction process of data [18] is based on what response is given from
 397 the detectors. It is affected by pile-up and the energy of that which is detected.
 398 This process is not specifically used in the thesis, however the smearing functions
 399 are discussed in section 2.1.

400 1.3.5 Pile-up

401 Pile-up is the phenomena that several proton-proton collisions occur simultaneously.
 402 The number of pile-up is defined as the average number of proton-proton
 403 collisions that occur per bunch crossing per second. It is denoted as $\langle \mu \rangle$. μ can
 404 be calculated by adjusting a Poisson distribution to fit the curve created by the
 405 number of interactions per bunch crossing at a given luminosity. When this is
 406 done μ will be the mean value of the Poisson distribution.

407 1.3.6 Mono-jet analysis

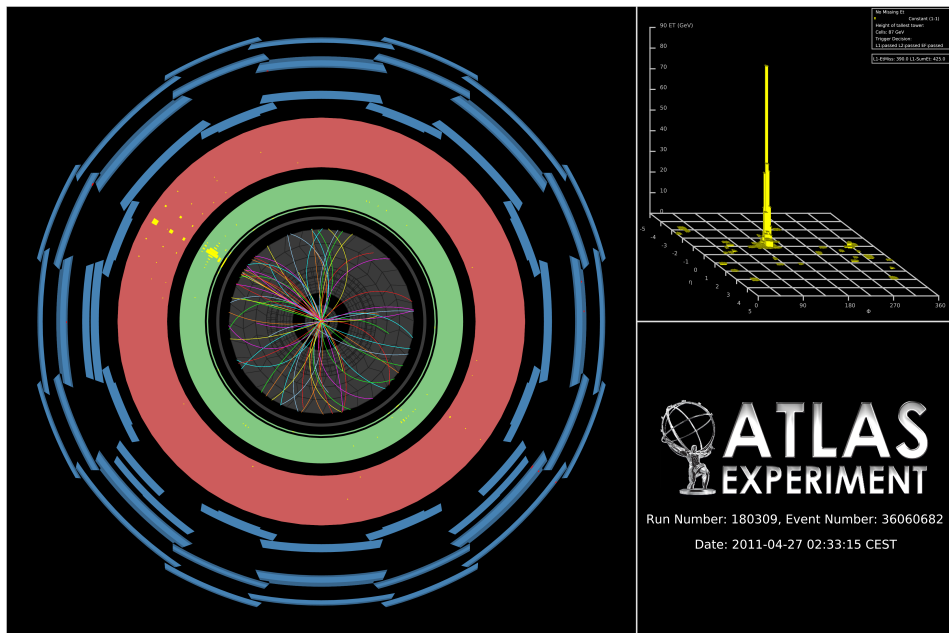


Figure 1.8: Image of an actual mono-jet event recorded by the ATLAS experiment [20].

408 When measuring the transversal energy one can in some interactions find incon-
 409 sistencies, such as jets that are in excess in one direction. In figure 1.8 one can see
 410 a high energetic jet which gives an excess of transversal energy in one direction
 411 after the collision. Since there is no balancing jet there must be transverse energy
 412 that is not detected, denoted E_T^{Miss} , since it was close to zero before the collision.
 413 This gives an indication that there energy to balance this that simply can not be
 414 detected. This could for instance be neutrinos or the sign of a new particle.

415 E_T^{Miss} is the modulus of the E_T^{Miss} vector which is defined as:

$$E_T^{\vec{M}iss} = -\sum E_T^{\vec{jet}} - \sum E_T^{\vec{Electron}} - \sum E_T^{\vec{\mu}on} - \sum E_T^{\vec{T}au} - \sum E_T^{\vec{\gamma}on} \quad (1.9)$$

416 Jets are hadrons which travel in the same direction and are usually created from

hadronization of a quark or a gluon in a collision. Usually jets are composed of a lot of energetic hadrons.

Since the jets are created from quarks or gluons, measuring a jet results in more information about the collision.

There are two main classes of events, signal and background. The signal corresponds to events that would arise from one of the processes in subsection 1.2.5. However to know that the missing energy is sign of the signal then one must understand all the other components that could contribute to the missing energy. Also there must be an excess of missing energy from what is expected from the background.

The background comprises of standard model processes that can mimic the mono-jet signature.

1.3.7 Phase II high luminosity upgrade

At the moment, the whole LHC is undergoing a step by step upgrade program which will be finalized around 2022-2023, denoted the high luminosity upgrade, or HL-upgrade. The upgrade consists of different stages, meaning that the upgrade will halt for periods so that experiments can take place. In figure 1.9 one can see

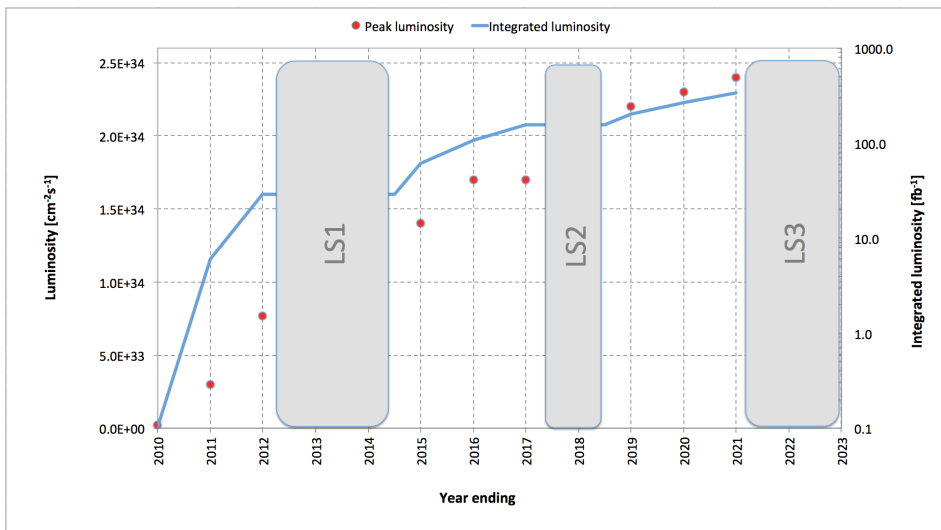


Figure 1.9: A graph showing the upgrading timetable with the instantaneous luminosity, denoted luminosity, and integrated luminosity expected in the different stages.

the three proposed upgrades. The period before LS1 is denoted phase 0, after LS1 and before LS2 phase I and after LS3 phase II.

LS1 is the upgrade which will take the LHC to its designed performance.

- 437 LS2 will take the LHC to the ultimate designed instantaneous luminosity.
 438 LS3 which is the focus of this thesis, will increase the instantaneous luminosity
 439 even more. Though for this to happen a modification of the whole LHC
 440 must be done, instead of just an upgrade and maintenance as before.

441 The following is expected for the experiments done after phase II:

Entity	Expected	Last run (2012)
Instantaneous luminosity	$\mathcal{L} \sim 50 \text{ nb}^{-1} \text{s}^{-1}$	$\mathcal{L} \sim 10 \text{ nb}^{-1} \text{s}^{-1}$
Integrated luminosity	$\mathcal{L} = 1000 - 3000 \text{ fb}^{-1}$	$\mathcal{L} = 20 \text{ fb}^{-1}$
Pile-up	$\langle \mu \rangle = 140$	$\langle \mu \rangle = 20$
Center of mass energy	$\sqrt{s} = 14 \text{ TeV}$	$\sqrt{s} = 8 \text{ TeV}$

Table 1.2: Expected running values for the Phase II HL-upgraded LHC with older values for comparison [21].

442 Where it should be noted that the integrated luminosity indicates the total amount
 443 of data which will be collected after the upgrade is completed before the next up-
 444 grade takes place.

445 1.3.8 Monte Carlo simulation

- 446 As mentioned before, in this thesis only emulated data has been used. This data
 447 is created by using a Monte Carlo (MC) simulation of the background processes
 448 and the expected signal. To do this a program called MadGraph is used.
 449 MadGraph [22] starts with Feynman diagrams and then generates simulated events
 450 based on lots of different parameters.
 451 PYTHIA [23] is a package which adds the correct description of jets to MadGraph
 452 by including hadronization. The correct description of pile-up comes from other
 453 ATLAS software.
 454 The tool to access all this data and analyse it a tool called ROOT, which is used
 455 for programming high energy physics related tools [24].

2

Validation of smearing functions

458 A full detector simulation of the ATLAS detector based on the GEANT [25] pro-
459 gram makes it possible to obtain the expected detector responses to electrons,
460 muons, tau leptons, photons (γ) and jets of hadrons. However these simulations
461 are extremely time-consuming and require a lot of computing power. Also at the
462 present time only a limited set of these simulations exists for the ATLAS phase II
463 upgrade.

464 In this thesis a different strategy is used. Instead of performing a full detector
465 simulation the observed particles from the event generator, which simulates the
466 proton-proton collisions, are smeared by using random numbers following reso-
467 lution functions specific to each type of particle. These emulate how the detector
468 and the reconstruction is affected by the increased luminosity and the pile-up
469 which comes with this.

470 The resolution functions or smearing functions are the official functions devel-
471 oped from previous studies [1, 26] by the ATLAS collaboration for the study of
472 the ATLAS phase II upgrade. The key feature of those studies was that the di-
473 rection of the momenta is unaffected and that only jets and E_T^{Miss} are affected by
474 pile-up. Since this was confirmed in previous studies it was not incorporated into
475 the smearing functions as discussed more in section 2.1.

476 Since part of this thesis work was to take the official ATLAS smearing functions
477 and apply the smearing to each particle, it was important to check that the en-
478 ergy and momenta resolutions of the smeared objects were consistent with the
479 expected values. Thus in this chapter the energy and momenta resolutions are
480 measured after applying the smearing to some simulated processes and the re-
481 sulting resolutions are compared with the expected values.

482 2.1 Smearing functions

483 These smearing functions are designed so that they take into account the effi-
 484 ciency of the different detectors, limitations as well as their dependence on pile-
 485 up. They also take into account how all this varies depending on the measured
 486 entries energy or momenta.

487 Terminology:

- 488 • Data before smearing, simulated data, is denoted as data at a truth level or
 489 truth data.
- 490 • Data after smearing, which is comparable to what is measured is denoted
 491 as reconstructed or reco data as discussed in subsection 1.3.4.

492 2.1.1 Electron and photon

493 The identification of electrons relies on finding an isolated electron track and
 494 a pattern in the calorimeter compatible with an electron shower. Pile-up will
 495 affect the electrons by decreasing the efficiency to identify an electron because of
 496 the increased number of tracks. However for the identified electrons the energy
 497 resolution will be close to that without pile-up.

498 The electron and photon have the same smearing since they are both detected in
 499 a similar way.

500 2.1.2 Muon

501 The identification of muons relies on isolated tracks in the inner detector being
 502 matched with information in the muon system. Since the muon system is the
 503 outer most detector seen from the collision point it is unaffected by the false
 504 detection effects of pile-up.

505 2.1.3 Tau

506 Tau is detected similarly to electron and photon. In this thesis all tau processes
 507 are assumed to be at 3 prong. Where prong refers to the different amount of
 508 tracks from which they were reconstructed. This in turn means that the effect of
 509 pile-up will be worse compared to an electron as a triplet must be found in an
 510 increased number of tracks.

511 2.1.4 Jets

512 The largest effect of pile-up is to add additional jets in the ATLAS detector. These
 513 additional jets contribute to additional energy deposited inside the existing jets
 514 and to E_T^{Miss} .

515 2.1.5 Missing Transversal Energy

516 E_T^{Miss} , the missing transversal energy, which was discussed in subsection 1.3.6,
 517 and defined in (1.9) is calculated by knowing that there should be energy conser-

518 vation in the collision. It is comprised of different parts, one from neutrinos, one
519 from errors in the other measurements and one from new physics. It should be
520 affected by pile-up as described above.

2.2 Validation

To validate the smearing functions a comparison with Ref. [26] was made where the standard deviation, depending on the energy or momentum value of an entity, was given, see section 2.4. This is performed using the simulated processes listed in table 2.1.

Table 2.1: Different processes from where data has been taken. Each sample is a simulation of a physical process, the simulation names can be found in appendix A

Particle	Process
Electron	$W \rightarrow e\nu$
Muon	$W \rightarrow \mu\nu$
Tau	$W \rightarrow \tau\nu$
γ	$\gamma + \text{Jet sample}$
Jets	Jet sample
E_T^{Miss}	$Z \rightarrow \nu\nu + \text{Jet sample}$

The energy and momentum resolutions are obtained for each type of particle by comparing the values before and after smearing. This is done looking at the reco data for a given truth energy or momentum value. Since the smearing functions takes a lot into account the match will not be a fine line as seen in figure 2.3b.

By fitting a Gaussian curve to this data will then result in the standard deviation which is used in the validation. The standard deviation is also known as the resolution of the data and will be denoted σ .

This resolution is then compared to previous results, [26].

To get enough statistics enough data must be available for a given truth energy or momenta and the analysis must be specific enough to only look at a narrow enough interval around this point.

537 **2.3 Results**

- 538 As discussed above, the method was to plot the data against its smeared counter-
539 part and through this determine σ to see if it conforms to the expected values.
- 540 Only one energy value is shown for simplicity, though the comparison was done
541 for different energy values.
- 542 The average number of pile-up is fixed at 60 as a benchmark unless anything else
543 is stated.
- 544 The images are, as the comparison, often divided depending on the different η
545 values.
- 546 All results are summarized in table 2.5.

547 2.3.1 Electron and photon

548 Since these interact very similarly in the detector, their smearing functions are
 549 identical. The slice value represents at which value of unsmeared energy or mo-
 550 mentum this smearing occurs.

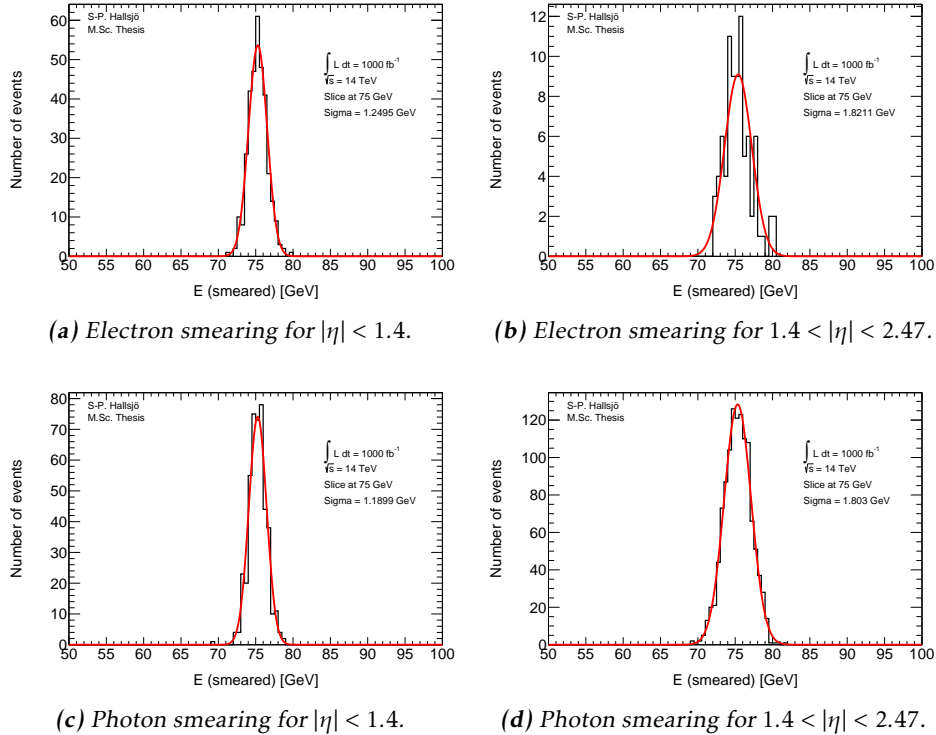


Figure 2.1: Photon and electron smearing plots.

551 **2.3.2 Muon**

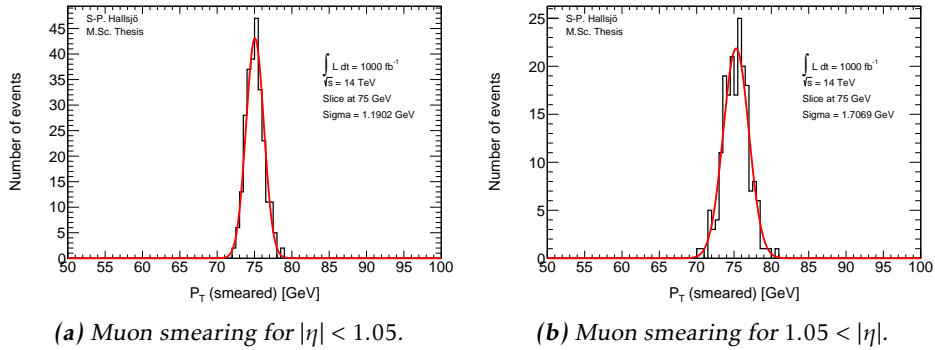


Figure 2.2: Muon smearing plots.

552 **2.3.3 Tau**

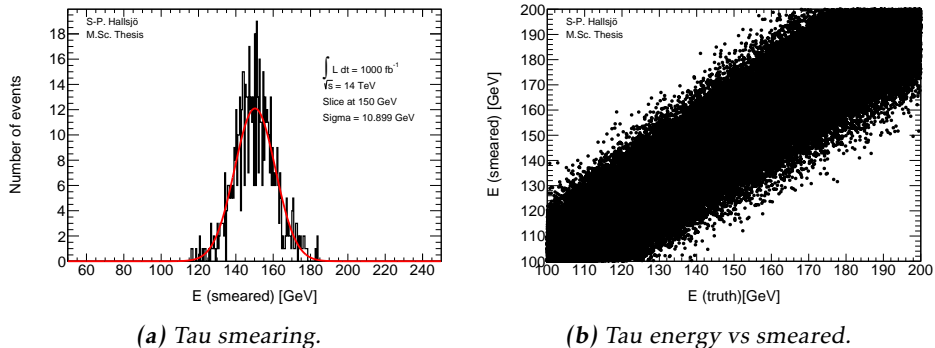


Figure 2.3: Tau smearing and energy vs smearing plot.

553 2.3.4 Jets

Jets as described in subsection 1.3.6, are hadronic showers. The smearing functions are divided into four different regions depending on the angle η .

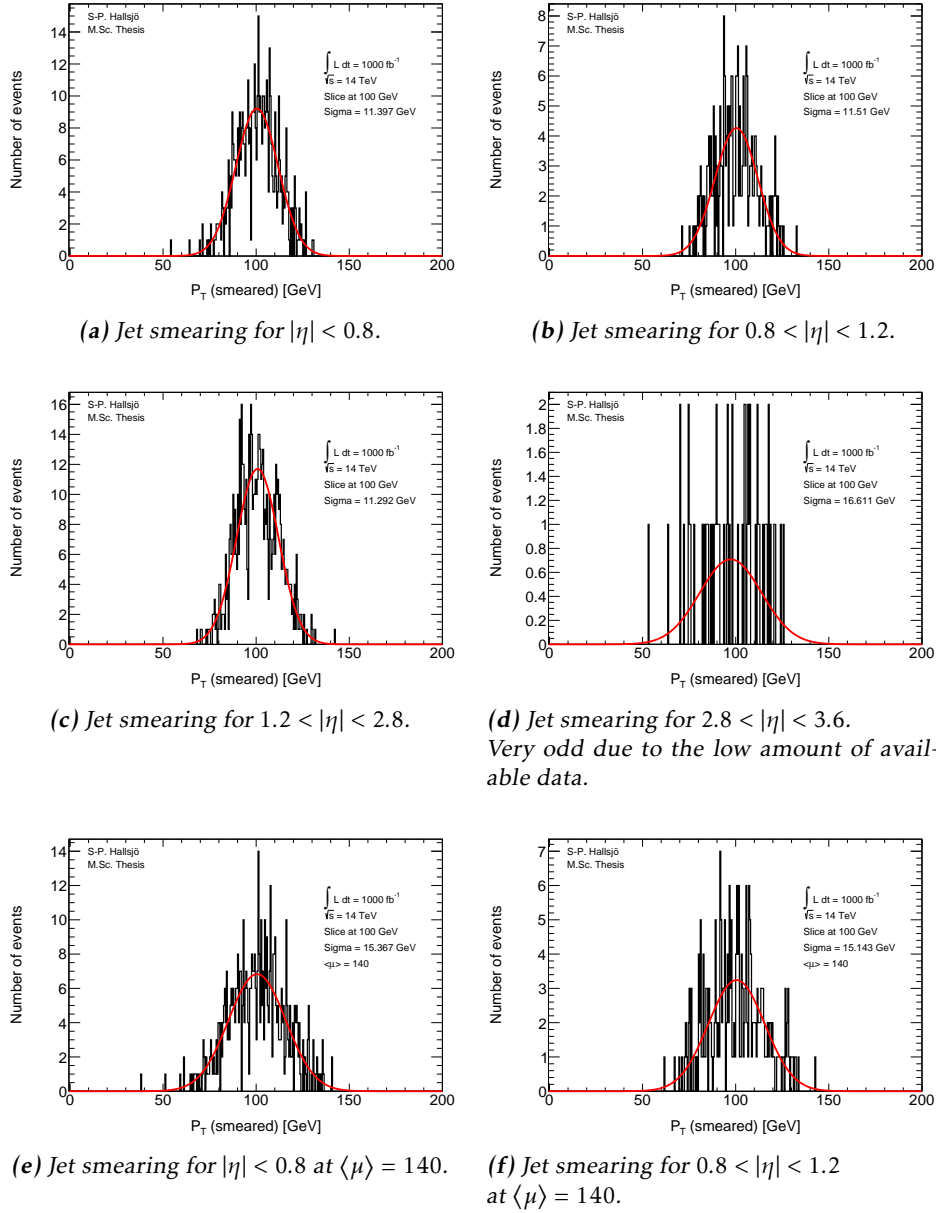


Figure 2.4: Jet smearing plots.

556 2.3.5 Missing Transversal Energy

557 These figures are given as smeared value from origin, thus at 0 it represents that
 558 the energy is unsmeared, compared to the others where the slice value represents
 559 the unsmeared.

560 Here the E_T^{Miss} is projected down to the x- and y-axis, since these are the transver-
 561 sal axes, to be smeared.

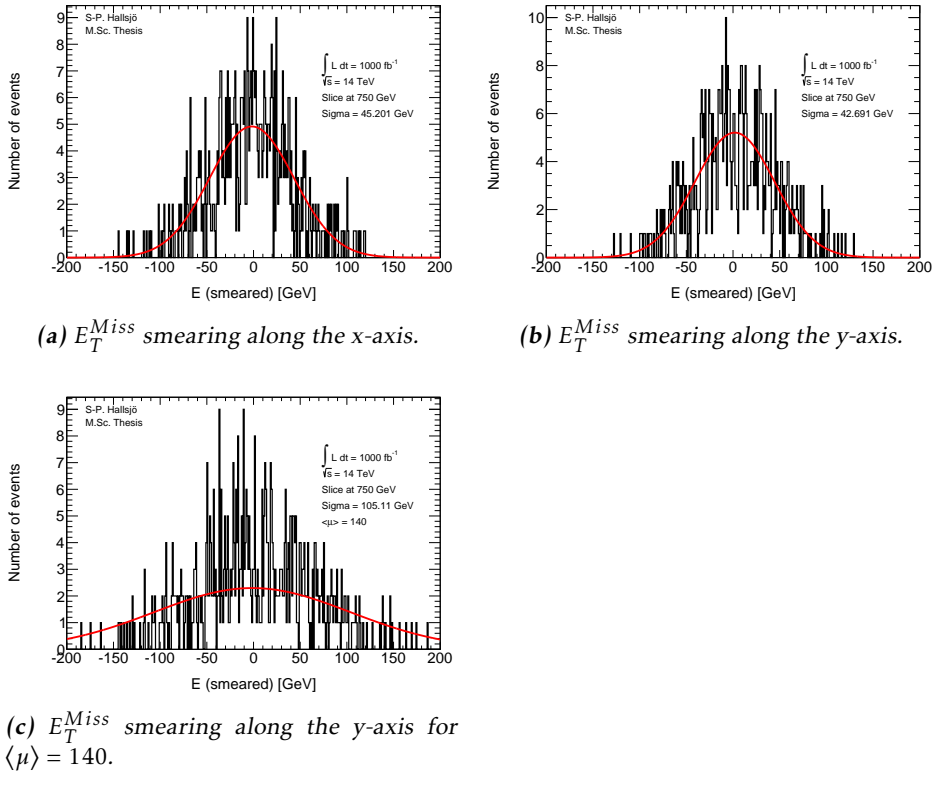


Figure 2.5: E_T^{Miss} smearing plots

562 2.4 Expected results

563 The expected response has been calculated and taken from [26].

564 The independence of pile-up for leptons and photons is backed up in previous
565 research, for instance [1, 27] were the first states:

566 “The uncertainty due to pile-up was investigated by comparing
567 simulated MC samples with and without pile-up and was found to be
568 negligible”

569 To validate the smearing code comparisons were made with [26] which gave the
570 following formulation for the expected σ :

Observable	Absolute σ
Electron & photon	$\sigma = 0.3 \oplus 0.1\sqrt{E(GeV)} \oplus 0.01E(GeV), \eta < 1.4$ $\sigma = 0.3 \oplus 0.15\sqrt{E(GeV)} \oplus 0.015E(GeV), 1.4 < \eta < 2.47$
Muon momentum	$\sigma = \frac{\sigma_{id}\sigma_{ms}}{\sigma_{id} \oplus \sigma_{ms}}$ $\sigma_{id} = P_T(a_1 \oplus a_2 P_T)$ $\sigma_{ms} = P_T(\frac{b_0}{P_T} \oplus b_1 \oplus b_2 P_T)$
Tau energy	$\sigma = (0.03 \oplus \frac{0.76}{\sqrt{E(GeV)}})E(GeV)$, for 3 prong.
Jet momentum	$\sigma = P_T(GeV)(\frac{N}{P_T} \oplus \frac{S}{\sqrt{P_T}} \oplus C)$ where $N = a(\eta) + b(\eta)\mu$
E_T^{Miss}	$\sigma = (0.4 + 0.09\sqrt{\mu})\sqrt{\sum E(GeV) + 20\mu}$

Table 2.2: Expected absolute σ where the parameters are given for muons in table 2.3 and for jets in table 2.4. Functions take from [26].

	a_1	a_2	b_0	b_1	b_2
$ \eta < 1.05$	0.01607	0.000307	0.24	0.02676	0.00012
$ \eta > 1.05$	0.03000	0.000387	0.00	0.03880	0.00016

Table 2.3: Parameters used in the muon smearing function taken from [26].

$ \eta $	a	b	s	C
0-0.8	3.2	0.07	0.74	0.05
0.8-1.2	3.0	0.07	0.81	0.05
1.2-2.8	3.3	0.08	0.54	0.05
2.8-3.6	2.8	0.11	0.83	0.05

Table 2.4: Parameters used in the jet smearing function taken from [26].

Process	σ [GeV]	Expected σ
Electron low η	1.24948 ± 0.0481987	1.18427
High η	1.8211 ± 0.141329	1.74446
Photon low η	1.18986 ± 0.0400187	1.18427
High η	1.80297 ± 0.0374312	1.744463
Muon low η	1.19016 ± 0.0524938	1.49789
High η	1.70694 ± 0.0882606	2.18318
Tau	10.8992 ± 0.299761	10.3388
Jet low η	11.3974 ± 0.351391	11.5983
$\langle\mu\rangle = 140$	15.3673 ± 0.473783	15.7721
Mid low η	11.5096 ± 0.518872	11.9352
$\langle\mu\rangle = 140$	15.1427 ± 0.682649	15.9515
Mid high η	11.2916 ± 0.310314	10.9439
High η	16.6112 ± 1.52891	13.5
E_T^{Miss} x-axis	45.2013 ± 1.35426	48.4483
E_T^{Miss} y-axis	42.6906 ± 2.27904	48.44834
$\langle\mu\rangle = 140$	105.109 ± 12.239	87.2812

Table 2.5: σ values.

- Where the given σ is still the absolute.
- Where the large difference between calculated and expected σ for Muons and E_T^{Miss} is explained by incorrectly calculated errors in σ .

571

572

573

574 2.5 Discussion

575 2.5.1 Smearing independent on pile-up

576 From the validation done it was interesting to note that the smearing functions
577 were created from previous studies, [1, 27], which had shown that leptons and
578 photons are not affected by pile-up. This may seem incredible however it be-
579 comes quite logical when one understands how the detectors work. To be able to
580 detect particles the detectors must detect an excess of energy which comes from
581 a particle passing through. This should not be distorted by an increased pile-up.
582 The amount of particles passing through will of course increase, but the detec-
583 tions should be unaffected as well as the recreation of the events. However with
584 the same logic it makes sense that jets and E_T^{Miss} are quite affected since they
585 are combined of several parts, either hadronic particles or by all the transversal
586 missing energy.

587 Another interesting part is how the effect diminishes with and increasing energy.
588 As seen above, and through the the formula, for the high energies which were of
589 interest here the effect is minimal.

590 2.5.2 Comparison to expected results

591 One of the major problems in the comparison was to get the significance of the
592 Gaussian fit to be calculated correctly. The tool ROOT has a lot of different fea-
593 tures which made this task somewhat difficult. Also since this is a statistical
594 property there is a statistical fluctuation in the result.

595 Another was to retrieve the correct values from the paper, [26], since it was un-
596 clear if the values given were absolute or scale dependent. This has now been
597 corrected in a new version of the paper.

598 **2.6 Conclusion**

- 599 The smearing functions work as intended within 5.8 sigma, however when using
600 a test box and averaging the sigmas one ends up with half of this for the extreme
601 cases, muons and E_T^{Miss} y-axis.

602

3

603

Evaluating dark matter signals

604 **Disclaimer: All data provided is still a work in progress and may be subject to
605 change before the final version.**

606 The main goal of the thesis is to investigate if certain dark matter signals can
607 be detected after the high luminosity upgrade. One immediate worry is that the
608 background will be large in comparison to the signal, making the signal undetectable.
609

610 The signal models are given in appendix A along with the background models.
611 The different models were discussed in part in subsection 1.2.5 and some more
612 in this chapter.

613 This thesis focus on using a luminosity at 1000 fb^{-1} and a center of mass energy
614 at 14 TeV. The reco data is created using a pile-up rate, $\langle \mu \rangle = 140$ as expected
615 during phase II.

616 Each of these has been evaluated in different signal regions and the detectability
617 has been evaluated using a statistical P-value. This process has been performed
618 at different pile-up values.

619 3.1 Signal to background ratio

620 3.1.1 Selection criteria

621 For different purposes different selection criteria or regions are used. These are a
 622 set of criteria specified to enhance the area of interest. For instance, if simulating
 623 a specific signal one wants to find as many ways as possible to diminish the back-
 624 ground. This so that when searching experimentally, the signal will be easier to
 625 detect.

626 These can be quite general cuts, there are only some things to take into consider-
 627 ation.

- 628 • If experimental, what limitations are set by the detectors? Are there some
 629 criteria already?
- 630 • If simulated, is there some criteria set in the generator?
- 631 • Are there criteria which must be set since there is to much uncertainty in
 632 the data? or a large effect of pile up?

633 3.1.2 Verifying background data

634 To verify that the background data was correct it was compared with Ref. [28]
 635 in which the center of mass energy is 8 TeV and the luminosity is 10 fb^{-1} . Since
 636 the luminosity is not 1000^{-1} as used in this thesis the expected values from the
 637 paper scaled up with a factor 100 to be comparable.

638 Somewhat unexpectedly a center of mass energy at 8 TeV required the cross-
 639 sections to be a factor 4 lower than the cross-sections at 14 TeV. **How do I ref-**
640 erence the cross-section?

The signal regions used in the article were the following:

Selection Criteria		
Jet veto, require no more than 2 jets with $p_T > 30 \text{ GeV}$ and $ \eta < 4.5$		
Lepton veto, no electron or muon		
Leading jet with $ \eta < 2.0$ and $\Delta\phi(\text{jet}, E_T^{\text{miss}}) > 0.5$ (second-leading jet)		
signal region	SR3p	SR4p
minimum leading jet p_T (GeV)	350	500
minimum E_T^{miss} (GeV)	350	500

Table 3.1: The signal regions from Ref. [28].

641
 642 The article had in total four signal regions, unfortunately since the simulated
 643 events used in this thesis are filtered before the analysis only the two highest
 644 regions are comparable. This can be seen in subsection 3.4.1 in table 3.3.

645 **3.1.3 Weight**

646 A weight is used to normalize different types of data so that they can be compared.
 647 In thesis the following is used:

$$648 \text{weight} = \frac{\mathcal{L}\sigma}{N_{Raw}} \quad (3.1)$$

648 where N_{Raw} is number of events expected at the luminosity that was set to create
 649 the data, compared to \mathcal{L} which is the luminosity at which the data is compared
 650 and σ is the cross-section.

651 **3.1.4 Figure of merit**

652 To be able to evaluate different signal regions and different signal models, a figure
 653 of merit p is used. The value p is the probability for an assumed hypothesis
 654 to be correct, thus a good signal region will yield a low value. The assumed
 655 hypothesis is that the background and its fluctuations is measured over the signal
 656 plus background.

657 Assuming the expected number of background events are $B \pm \sigma_B$ where σ_B is the
 658 quadratic sum of the statistical error from Monte Carlo, the statistical error from
 659 the control region (CR) and the systematic errors. The expected number of signals
 660 is S , assumed without fluctuation.

661 If no uncertainty in B or S is assumed, then the number of expected events, N , in
 662 the signal region should follow a Poisson distribution as such:

$$663 P(N|S+B) = \frac{e^{-(S+B)}(S+B)^N}{N!} \quad (3.2)$$

663 However since there is an uncertainty in the background, the probability distri-
 664 bution $P(N|S+B)$ must be convoluted with a Gaussian function:

$$665 G(N_B|B, \sigma_B) = \frac{1}{\sigma_B \sqrt{2\pi}} e^{-\frac{(N_B-B)^2}{2\sigma_B^2}} \quad (3.3)$$

where N_B is the expected number of background events. The convolution is done
 using N_B as N resulting in the total probability density function:

$$666 F(N|S+B, \sigma_B) = P(N|S+N_B)*G(N_B|B, \sigma_B) = \\ = \int_{-\infty}^{\infty} P(N|N_B - (S+B))G(N_B|B, \sigma_B)dN_B \quad (3.4)$$

665 This leads to the probability of the signal plus background fluctuation to B events
 666 being obtained by summing the probability function from $N=0$ to $N=B$.

$$667 p = \sum_{i=0}^B \int_{-\infty}^{\infty} P(i|N_B - (S+B))G(N_B|B, \sigma_B)dN_B \quad (3.5)$$

In this thesis, two different models of the error in the background σ_B are used. Both models are based on Ref. [28]. As described in the beginning of this subsection the error is calculated as:

$$\sigma_B = \text{Statistical error from MC} \oplus \text{Statistical error in CR} \oplus \text{Systematic error}$$

- The statistical error from MC has been neglected since there is no way of estimating it for the used data.
- The statistical error from background CR has been assumed to decrease with the increased luminosity, $\frac{30}{380} \frac{\sqrt{L_{old}}}{\sqrt{L_{new}}}$
- The systematic error has been given two different values, from the article: $\frac{30}{380}$ or fixed at 0.02.
- All this results the total error being used as either, 0.0793411 or 0.0215018.

3.1.5 D5 operators

As described in the introduction subsection 1.2.5, one of the signals is modelled using the D5 operator. In this thesis two different scenarios were used, one at a dark matter mass of 50 GeV and one at 400 GeV.

Discuss M^* , and the difference in mDM.

Was discussed in part in

What does M_S mean? M_S or M^* given in GeV. It is the suppression given to the probability of the process.

Why does one want to find limits on M^* ? How much can it be suppressed and still detectable.

3.1.6 Light vector mediator models

Discuss M_m , width, and the difference in mDM.

As described in the introduction subsection 1.2.5, the other signal model is a vector mediator model. The data available is: two different widths $M_m/3$ and $M_m/8\pi$, where M_m denotes the mediator mass and **the width is ?** two different mDM, 50 GeV and 400 GeV and finally a variety of mediator masses.

690 3.2 Other selection criteria

691 3.2.1 Criteria

692 To be able to compare signal results to previous papers new signal regions were
 693 devised. It was also discovered that the requirement of no electrons was to harsh
 694 for the signal models. Because of this new signal criteria were devised.

Selection Criteria					
Jet veto, require no more than 2 jets with $p_T > 30\text{GeV}$ and $ \eta < 4.5$					
Lepton veto, no electron or muon.					
The electron veto is defined: $\Delta R(jet^{lead}, electron^{lead}) \geq 0.4$ and $electron^{lead} p_T > 20\text{GeV}$ removed.					
signal region	SR1	SR1p	SR2	SR3	SR4
minimum leading jet p_T (GeV)	350	500	600	800	1000
minimum E_T^{Miss} (GeV)	350	500	600	800	1000
signal region	SRa		SRb	SRc	SRd
minimum leading jet p_T (GeV)	350		350	350	350
minimum E_T^{Miss} (GeV)	350		600	800	1000

Table 3.2: The new signal regions

695 3.2.2 Verifying background data

696 To make sure that the altered electron veto still produces results comparable with
 697 [28] a comparison was made again. This can be seen in subsection 3.4.1 in ta-
 698 ble 3.4.

699 3.3 Mitigating the effect of the high luminosity

700 As discussed in subsection 2.5.1 the effect of pile-up should be minimal in the
701 high energy regions which are of interest in this thesis.

702 Mention that the effect is on a trigger level, that the lowest SR will be lost.

703 Even though this was envisioned as the primary focus of the thesis, it was shown
704 that the effect of pile-up is minute for these high signal regions. Thus the focus
705 was shifted to perform a more in-depth mono-jet analysis of different DM signal
706 models.

707 3.4 Results

708 3.4.1 Verifying background data

709 In table 3.3 a comparison has been made. It can be seen that the simulated events
 710 and expected events coincide on all accounts apart from $W \rightarrow \tau\nu$, $W \rightarrow \mu\nu$ and
 711 thus the total as well. **This can be explained by better separation of μ, τ and**
 712 **missing energy.** Tau can not be reconstructed as jets in the code, they can in
 713 reality!

714 Here used truth data as to not be effected by pile-up.

Process	SR3p	Expected SR3p	SR4p	Expected SR4p
$Z \rightarrow \nu\nu$	140298	152000	25250.3	27000
$W \rightarrow \tau\nu$	40700.8	37000	5861.74	3900
$W \rightarrow e\nu$	11229	11200	1506.58	1600
$W \rightarrow \mu\nu$	13727.1	15800	1872.32	4200
Total background	205955	218000	34491	36700

Table 3.3: Comparison of the simulated and expected events from [28] with $\mathcal{L} = 1000\text{fb}^{-1}$ and cross-sections corresponding to $\sqrt{s} = 8\text{TeV}$.

Process	SR1	Expected SR1	SR1p	Expected SR1p
$Z \rightarrow \nu\nu$	147009	152000	26734	27000
$W \rightarrow \tau\nu$	44727.7	37000	6543.82	3900
$W \rightarrow e\nu$	17964	11200	2470.46	1600
$W \rightarrow \mu\nu$	14285.7	15800	1971.87	4200
Total background	223986	218000	37720.2	36700

Table 3.4: Comparison of the simulated and expected events from [28] with $\mathcal{L} = 1000\text{fb}^{-1}$ and cross-sections corresponding to $\sqrt{s} = 8\text{TeV}$.

715 3.4.2 Events

- 716 Give a table with the number of events for signals and background in all signal
 717 regions both truth and reco.
- 718 The below is only for truth, must create new code to write it for reco.
- 719 Have a table with the number of signal and bkg ground events for the different
 720 SR where the signal then is given at $M^* 1\text{ GeV}$ for a good comparison.
- 721 Same tables as above but at reco.

Process	SR1	SR2	SR3	SR4
D5 mDm=50 $Q_{cut} = 200$	50410.4	0	0	0
M*=1TeV $Q_{cut} = 400$	53242.1	4934.73	0	0
$Q_{cut} = 600$	26210.6	25284.7	10749.7	4391.35
Total signal	129863	30219.4	10749.7	4391.35
Z $\rightarrow \nu\nu$	604479	42656.5	8423.89	2110.55
W $\rightarrow \tau\nu$	154140	7807.06	1307.89	295.124
W $\rightarrow e\nu$	61771.6	2890.39	485.485	109.887
W $\rightarrow \mu\nu$	49114.3	2357.17	379.201	90.9721
Total background	869505	55711.2	10596.5	2606.54

Table 3.5: Signal and background events for truth data in the signal regions.

Process	SRa	SRb	SRc	SRd
Signal 1 $Q_{cut} = 200$	50410.4	434.012	0	0
Signal 1 $Q_{cut} = 400$	53242.1	10018.1	159.539	22.0054
Signal 1 $Q_{cut} = 600$	26210.6	25958.1	12767.2	5199.47
Signal 1 total	129863	36410.1	12926.8	5221.48
Z $\rightarrow \nu\nu$	604479	58613.9	11383.4	2842.85
W $\rightarrow \tau\nu$	154140	10678.5	1788.16	385.861
W $\rightarrow e\nu$	61771.6	3961.35	653.918	152.221
W $\rightarrow \mu\nu$	49114.3	3051.61	498.995	108.086
Total background	869505	76305.4	14324.5	3489.02

Table 3.6: Signal and background events for truth data in the signal regions.

3.4.3 Limit on M*

The mass suppression scale.

Give at 1000fb-1 and with 14 TeV cross-sections. And for the different signal regions. Refer to M* explained in subsection d5.

For the new signal regions: **Include a table of the limits for truth and Reco.**

Process	SR1	SR2	SR3	SR4
Signal 1 $Q_{cut} = 200$	41968.9	0	0	0
Signal 1 $Q_{cut} = 400$	52235.9	4126.01	0	0
Signal 1 $Q_{cut} = 600$	26090	23893	9978.04	4130.4
Signal 1 total	120295	28019	9978.04	4130.4
$Z \rightarrow \nu\nu$	553735	39104.6	7680.99	1932.33
$W \rightarrow \tau\nu$	156023	7741.1	1282.23	275.877
$W \rightarrow e\nu$	58873.9	2705.75	447.655	106.284
$W \rightarrow \mu\nu$	47800.6	2298.63	380.102	89.1707
Total background	816433	51850	9790.98	2403.66

Table 3.7: Signal and background events for reco data with $\langle \mu \rangle = 140$ in the signal regions.

Process	SRa	SRb	SRc	SRd
Signal 1 $Q_{cut} = 200$	41968.9	564.215	0	0
Signal 1 $Q_{cut} = 400$	52235.9	13131.8	275.068	22.0054
Signal 1 $Q_{cut} = 600$	26090	25065.8	13477.1	5482.88
Signal 1 total	120295	38761.9	13752.2	5504.88
$Z \rightarrow \nu\nu$	553735	71613.2	13145.1	3139.89
$W \rightarrow \tau\nu$	156023	14500.3	2174.02	467.433
$W \rightarrow e\nu$	58873.9	5177.33	789.925	175.639
$W \rightarrow \mu\nu$	47800.6	4030.7	617.889	138.71
Total background	816433	95321.6	16727	3921.67

Table 3.8: Signal and background events for reco data with $\langle \mu \rangle = 140$ in the signal regions.

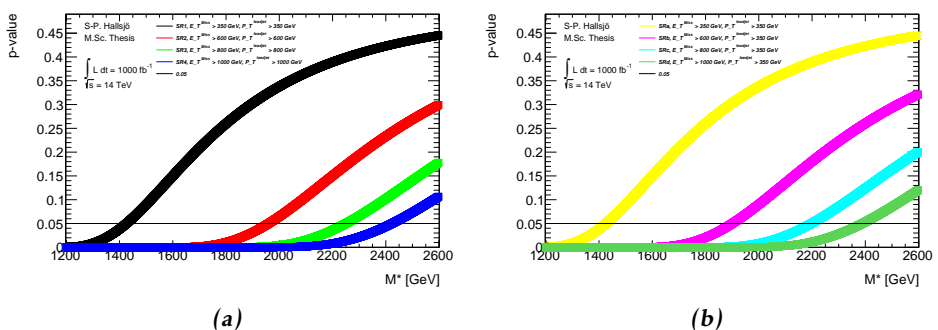


Figure 3.1: On a truth level error model 0.02.

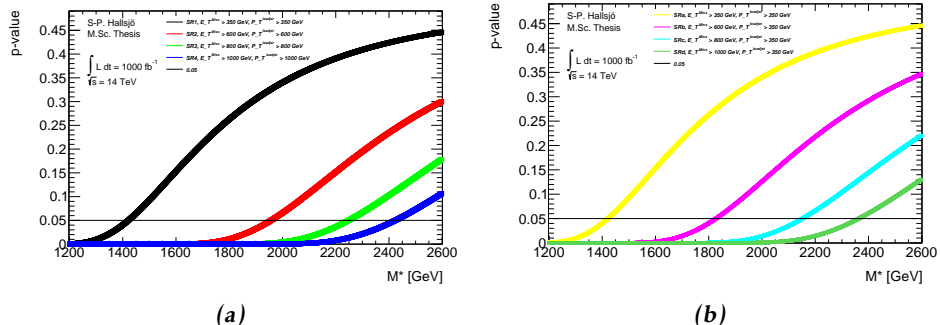


Figure 3.2: On a reco level error model 0.02.

Signal region	Mass suppression scale Truth data	Reco data
SR1	1425	1420
SR2	1960	1957
SR3	2249	2248
SR4	2423	2423
SRa	1425	1421
SRb	1900	1827
SRc	2197	2152
SRd	2389	2363

Table 3.9: Mass suppression scales in GeV given for the 0.02 error model.

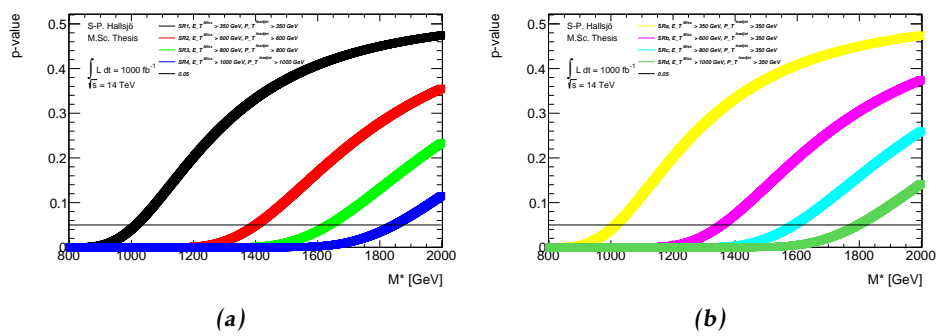


Figure 3.3: On a truth level error model 0.10.

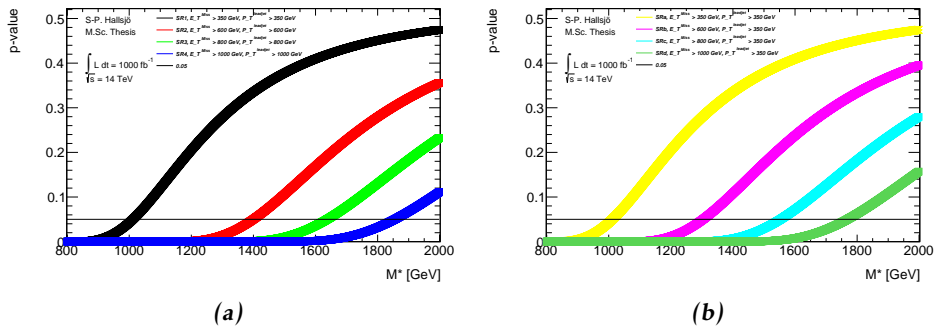


Figure 3.4: On a reco level error model 0.10.

Signal region	Mass suppression scale Truth data	Reco data
SR1	1015	1012
SR2	1400	1400
SR3	1636	1637
SR4	1846	1854
SRa	1015	1012
SRb	1356	1303
SRC	1589	1553
SRd	1796	1768

Table 3.10: Mass suppression scales in GeV given for the 0.10 error model.

727 3.4.4 Effect of pile-up on M^*

728 Hardly any effect. 10 % or in that vicinity.

729 3.4.5 Previous results

730 10fb paper. Preliminary not that much better results for 1000fb-1 and 14TeV.

731 The whole discussion with Steven and David.

732 3.4.6 Limit on mediator mass

733 Are there previous results? Signal vs background plot in normal and log scale for
 734 one of the vector mediator models, to be able to evaluate all the different models
 735 the so called p-value was used in different signal regions. Below are two figures
 736 showing one of the vector mediator models in SR3.

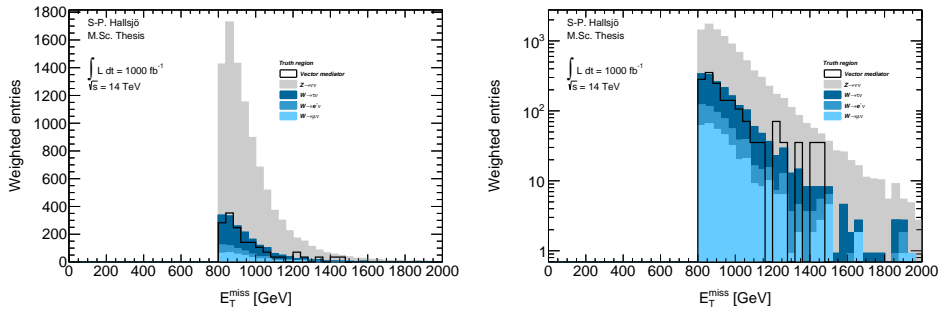


Figure 3.5: Signal on background plot to illustrate the a general plot.

To set a limit on the mediator mass the p-value was calculated in different signal regions for the different signal models with different mediator mass. This resulted in the following plot:

3.4.7 Effect of pile-up on mediator mass

Check the different cases for reco and truth to see what happens.

742 3.5 Discussion**743 3.5.1 Comparison to previous results****744 3.5.2 Effect of the high luminosity**

745 3.6 Conclusion

746 3.6.1 Limit on M^*

747 3.6.2 Limit on mediator mass

748

4

749

Results and Conclusions

750 **Disclaimer: This chapter not yet completed.**

751 4.1 Validation of smearing functions

752 Have some discussion.

753 Result they appear to work as expected, the reference paper was a bit unclear, I
754 leave my writing as a better reference.

755 4.2 Signal to background ratio

756 4.2.1 Limit on M*

757 4.2.2 Limit on mediator mass

758 4.3 Other selection criteria and observables

759 4.3.1 Limit on M*

760 4.3.2 Limit on mediator mass

761 4.4 Mitigating the effect of the high luminosity

762 4.5 Recommendations to mitigate the effect of the 763 high luminosity

764 Keep to a higher energy region, or signal region.

765 4.6 Suggestions for future research

766 With more time, search for new signal regions, the only solution now for the HL
767 is to go up in energy. Since none of the other parameters (eta,phi etc) seem to be
768 altered these can not be used. Is there something that has been overlooked?

769 Test the effect of pile-up for lower signal regions? See if the effect is as great as
770 predicted.

771 Explore other theoretical models for dark matter, other d operators etc. Models
772 that are based on Supersymmetry and not just effective theories.

773 Sätt av ett kort kapitel sist i rapporten till att avrunda och föreslå räkningar för
774 framtida utveckling av arbetet.

775 Saving as reference. test citing as: Here we cite Duck [29] [29].

776 If the above works, remember to edit myreferences.

Appendix

778

A

779

Datasets

780 A.1 Background processes

781 A.1.1 Validation

782 For the validation the following datasets were used, with a filter at generator level
783 at 450GeV for lead jet and MET.

784 mc12.157539.sherpa_ct10_znunupt280d4pd.v03 mc12.157534.sherpa_ct10_wenupt200d4pd.v03

785 mc12.157535.sherpa_ct10_wmunupt200d4pd.v03

786 mc12.157536.sherpa_ct10_wtaunupt200d4pd.v03

787 mc12.129160.pythia8_au2cteq6l1_perf_jf17d4pd.v03

788 mc12.129160.pythia8_au2cteq6l1_perf_jf17d4pd.v04

789 mc12.129170.pythia8_au2cteq6l1_gammajet_dp17d4pd.v04

790 They should be read as such: Monte Carlo version, dataset number, generator, ?
791 name.

793 A.1.2 Background to signals

794 The same as the above though now with the filter as indicated by their name. The
795 second znunu sample has been generated with and center of mass energy at 8
796 TeV.

797 mc12.157539.sherpa_ct10_znunupt280d4pd.v05

798 mc12.157539.8tev_sherpa_ct10_znunupt280d4pd.v05

799 mc12.157536.sherpa_ct10_wtaunupt200d4pd.v05

800 mc12.157534.sherpa_ct10_wenupt200d4pd.v05

801 mc12.157535.sherpa_ct10_wmunupt200d4pd.v05

802 A.2 Signals

803 A.2.1 Qcut

804 Qcut means that the original data has been split into different parts depending
 805 on the value of the lead jet pt.

806 A.2.2 D5 signal processes

```
807 mc12.188408.madgraphpythia_auet2bcteq6l1_d5_dm50_ms10000_
808 qcut200d4pd.v06
809 mc12.188409.madgraphpythia_auet2bcteq6l1_d5_dm50_ms10000_
810 qcut400d4pd.v06
811 mc12.188410.madgraphpythia_auet2bcteq6l1_d5_dm50_ms10000_
812 qcut600d4pd.v06

813 mc12.188411.madgraphpythia_auet2bcteq6l1_d5_dm400_ms10000_
814 qcut200d4pd.v06
815 mc12.188412.madgraphpythia_auet2bcteq6l1_d5_dm400_ms10000_
816 qcut400d4pd.v06
817 mc12.188413.madgraphpythia_auet2bcteq6l1_d5_dm400_ms10000_
818 qcut600d4pd.v06
```

819 All signals should be read as such: Monte Carlo version, dataset number, generator,
 820 ?, name of operator, dark matter mass, default mass suppression scale,
 821 qcut part. As discussed in reference

822

823 A.2.3 Light vector mediator processes

```
824 mc12.188414.madgraphpythia_auet2bcteq6l1_dmv_dm50_mm100_w3_
825 qcut200d4pd.v06
826 mc12.188422.madgraphpythia_auet2bcteq6l1_dmv_dm50_mm100_w3_
827 qcut400d4pd.v06
828 mc12.188430.madgraphpythia_auet2bcteq6l1_dmv_dm50_mm100_w3_
829 qcut600d4pd.v06

830 mc12.188415.madgraphpythia_auet2bcteq6l1_dmv_dm50_mm300_w3_
831 qcut200d4pd.v06
832 mc12.188423.madgraphpythia_auet2bcteq6l1_dmv_dm50_mm300_w3_
833 qcut400d4pd.v06
834 mc12.188431.madgraphpythia_auet2bcteq6l1_dmv_dm50_mm300_w3_
835 qcut600d4pd.v06

836 mc12.188416.madgraphpythia_auet2bcteq6l1_dmv_dm50_mm500_w3_
837 qcut200d4pd.v06
838 mc12.188424.madgraphpythia_auet2bcteq6l1_dmv_dm50_mm500_w3_
839 qcut400d4pd.v06
```

```
840 mc12.188432.madgraphpythia_auet2bcteq6l1_dmv_dm50_mm500_w3_
841 qcut600d4pd.v06
842 mc12.188417.madgraphpythia_auet2bcteq6l1_dmv_dm50_mm1000_w3_
843 qcut200d4pd.v06
844 mc12.188425.madgraphpythia_auet2bcteq6l1_dmv_dm50_mm1000_w3_
845 qcut400d4pd.v06
846 mc12.188433.madgraphpythia_auet2bcteq6l1_dmv_dm50_mm1000_w3_
847 qcut600d4pd.v06
848 mc12.188418.madgraphpythia_auet2bcteq6l1_dmv_dm50_mm3000_w3_
849 qcut200d4pd.v06
850 mc12.188426.madgraphpythia_auet2bcteq6l1_dmv_dm50_mm3000_w3_
851 qcut400d4pd.v06
852 mc12.188434.madgraphpythia_auet2bcteq6l1_dmv_dm50_mm3000_w3_
853 qcut600d4pd.v06
854 mc12.188419.madgraphpythia_auet2bcteq6l1_dmv_dm50_mm6000_w3_
855 qcut200d4pd.v06
856 mc12.188427.madgraphpythia_auet2bcteq6l1_dmv_dm50_mm6000_w3_
857 qcut400d4pd.v06
858 mc12.188435.madgraphpythia_auet2bcteq6l1_dmv_dm50_mm6000_w3_
859 qcut600d4pd.v06
860 mc12.188420.madgraphpythia_auet2bcteq6l1_dmv_dm50_mm10000_w3_
861 qcut200d4pd.v06
862 mc12.188428.madgraphpythia_auet2bcteq6l1_dmv_dm50_mm10000_w3_
863 qcut400d4pd.v06
864 mc12.188436.madgraphpythia_auet2bcteq6l1_dmv_dm50_mm10000_w3_
865 qcut600d4pd.v06
866 mc12.188421.madgraphpythia_auet2bcteq6l1_dmv_dm50_mm15000_w3_
867 qcut200d4pd.v06
868 mc12.188429.madgraphpythia_auet2bcteq6l1_dmv_dm50_mm15000_w3_
869 qcut400d4pd.v06
870 mc12.188437.madgraphpythia_auet2bcteq6l1_dmv_dm50_mm15000_w3_
871 qcut600d4pd.v06
872 mc12.188438.madgraphpythia_auet2bcteq6l1_dmv_dm50_mm100_w8pi_
873 qcut200d4pd.v06
874 mc12.188446.madgraphpythia_auet2bcteq6l1_dmv_dm50_mm100_w8pi_
875 qcut400d4pd.v06
876 mc12.188454.madgraphpythia_auet2bcteq6l1_dmv_dm50_mm100_w8pi_
877 qcut600d4pd.v06
878 mc12.188439.madgraphpythia_auet2bcteq6l1_dmv_dm50_mm300_w8pi_
879 qcut200d4pd.v06
880 mc12.188447.madgraphpythia_auet2bcteq6l1_dmv_dm50_mm300_w8pi_
881 qcut400d4pd.v06
```

```
882 mc12.188455.madgraphpythia_auet2bcteq6l1_dmv_dm50_mm300_w8pi_
883 qcut600d4pd.v06
884 mc12.188440.madgraphpythia_auet2bcteq6l1_dmv_dm50_mm500_w8pi_
885 qcut200d4pd.v06
886 mc12.188448.madgraphpythia_auet2bcteq6l1_dmv_dm50_mm500_w8pi_
887 qcut400d4pd.v06
888 mc12.188456.madgraphpythia_auet2bcteq6l1_dmv_dm50_mm500_w8pi_
889 qcut600d4pd.v06
890 mc12.188441.madgraphpythia_auet2bcteq6l1_dmv_dm50_mm1000_w8pi_
891 qcut200d4pd.v06
892 mc12.188449.madgraphpythia_auet2bcteq6l1_dmv_dm50_mm1000_w8pi_
893 qcut400d4pd.v06
894 mc12.188457.madgraphpythia_auet2bcteq6l1_dmv_dm50_mm1000_w8pi_
895 qcut600d4pd.v06
896 mc12.188442.madgraphpythia_auet2bcteq6l1_dmv_dm50_mm3000_w8pi_
897 qcut200d4pd.v06
898 mc12.188450.madgraphpythia_auet2bcteq6l1_dmv_dm50_mm3000_w8pi_
899 qcut400d4pd.v06
900 mc12.188458.madgraphpythia_auet2bcteq6l1_dmv_dm50_mm3000_w8pi_
901 qcut600d4pd.v06
902 mc12.188444.madgraphpythia_auet2bcteq6l1_dmv_dm50_mm10000_w8pi_
903 qcut200d4pd.v06
904 mc12.188452.madgraphpythia_auet2bcteq6l1_dmv_dm50_mm10000_w8pi_
905 qcut400d4pd.v06
906 mc12.188460.madgraphpythia_auet2bcteq6l1_dmv_dm50_mm10000_w8pi_
907 qcut600d4pd.v06
908 mc12.188445.madgraphpythia_auet2bcteq6l1_dmv_dm50_mm15000_w8pi_
909 qcut200d4pd.v06
910 mc12.188453.madgraphpythia_auet2bcteq6l1_dmv_dm50_mm15000_w8pi_
911 qcut400d4pd.v06
912 mc12.188461.madgraphpythia_auet2bcteq6l1_dmv_dm50_mm15000_w8pi_
913 qcut600d4pd.v06
914 mc12.188462.madgraphpythia_auet2bcteq6l1_dmv_dm400_mm500_w3_
915 qcut200d4pd.v06
916 mc12.188468.madgraphpythia_auet2bcteq6l1_dmv_dm400_mm500_w3_
917 qcut400d4pd.v06
918 mc12.188474.madgraphpythia_auet2bcteq6l1_dmv_dm400_mm500_w3_
919 qcut600d4pd.v06
920 mc12.188463.madgraphpythia_auet2bcteq6l1_dmv_dm400_mm1000_w3_
921 qcut200d4pd.v06
922 mc12.188469.madgraphpythia_auet2bcteq6l1_dmv_dm400_mm1000_w3_
923 qcut400d4pd.v06
```

```
924 mc12.188475.madgraphpythia_auet2bcteq6l1_dmv_dm400_mm1000_w3_
925 qcut600d4pd.v06

926 mc12.188464.madgraphpythia_auet2bcteq6l1_dmv_dm400_mm3000_w3_
927 qcut200d4pd.v06
928 mc12.188470.madgraphpythia_auet2bcteq6l1_dmv_dm400_mm3000_w3_
929 qcut400d4pd.v06
930 mc12.188476.madgraphpythia_auet2bcteq6l1_dmv_dm400_mm3000_w3_
931 qcut600d4pd.v06

932 mc12.188465.madgraphpythia_auet2bcteq6l1_dmv_dm400_mm6000_w3_
933 qcut200d4pd.v06
934 mc12.188471.madgraphpythia_auet2bcteq6l1_dmv_dm400_mm6000_w3_
935 qcut400d4pd.v06
936 mc12.188477.madgraphpythia_auet2bcteq6l1_dmv_dm400_mm6000_w3_
937 qcut600d4pd.v06

938 mc12.188466.madgraphpythia_auet2bcteq6l1_dmv_dm400_mm10000_w3_
939 qcut200d4pd.v06
940 mc12.188472.madgraphpythia_auet2bcteq6l1_dmv_dm400_mm10000_w3_
941 qcut400d4pd.v06
942 mc12.188478.madgraphpythia_auet2bcteq6l1_dmv_dm400_mm10000_w3_
943 qcut600d4pd.v06

944 mc12.188467.madgraphpythia_auet2bcteq6l1_dmv_dm400_mm15000_w3_
945 qcut200d4pd.v06
946 mc12.188473.madgraphpythia_auet2bcteq6l1_dmv_dm400_mm15000_w3_
947 qcut400d4pd.v06
948 mc12.188479.madgraphpythia_auet2bcteq6l1_dmv_dm400_mm15000_w3_
949 qcut600d4pd.v06

950 mc12.188480.madgraphpythia_auet2bcteq6l1_dmv_dm400_mm500_w8pi_
951 qcut200d4pd.v06
952 mc12.188486.madgraphpythia_auet2bcteq6l1_dmv_dm400_mm500_w8pi_
953 qcut400d4pd.v06
954 mc12.188492.madgraphpythia_auet2bcteq6l1_dmv_dm400_mm500_w8pi_
955 qcut600d4pd.v06

956 mc12.188481.madgraphpythia_auet2bcteq6l1_dmv_dm400_mm1000_w8pi_
957 qcut200d4pd.v06
958 mc12.188487.madgraphpythia_auet2bcteq6l1_dmv_dm400_mm1000_w8pi_
959 qcut400d4pd.v06
960 mc12.188493.madgraphpythia_auet2bcteq6l1_dmv_dm400_mm1000_w8pi_
961 qcut600d4pd.v06

962 mc12.188482.madgraphpythia_auet2bcteq6l1_dmv_dm400_mm3000_w8pi_
963 qcut200d4pd.v06
964 mc12.188488.madgraphpythia_auet2bcteq6l1_dmv_dm400_mm3000_w8pi_
965 qcut400d4pd.v06
```

```
966 mc12.188494.madgraphpythia_auet2bcteq6l1_dmv_dm400_mm3000_w8pi_
967 qcut600d4pd.v06
968 mc12.188483.madgraphpythia_auet2bcteq6l1_dmv_dm400_mm6000_w8pi_
969 qcut200d4pd.v06
970 mc12.188489.madgraphpythia_auet2bcteq6l1_dmv_dm400_mm6000_w8pi_
971 qcut400d4pd.v06
972 mc12.188495.madgraphpythia_auet2bcteq6l1_dmv_dm400_mm6000_w8pi_
973 qcut600d4pd.v06
974 mc12.188484.madgraphpythia_auet2bcteq6l1_dmv_dm400_mm10000_w8pi_
975 qcut200d4pd.v06
976 mc12.188490.madgraphpythia_auet2bcteq6l1_dmv_dm400_mm10000_w8pi_
977 qcut400d4pd.v06
978 mc12.188496.madgraphpythia_auet2bcteq6l1_dmv_dm400_mm10000_w8pi_
979 qcut600d4pd.v06
980 mc12.188485.madgraphpythia_auet2bcteq6l1_dmv_dm400_mm15000_w8pi_
981 qcut200d4pd.v06
982 mc12.188491.madgraphpythia_auet2bcteq6l1_dmv_dm400_mm15000_w8pi_
983 qcut400d4pd.v06
984 mc12.188497.madgraphpythia_auet2bcteq6l1_dmv_dm400_mm15000_w8pi_
985 qcut600d4pd.v06
```

Bibliography

- [1] Collaboration ATLAS. Letter of Intent for the Phase-II Upgrade of the ATLAS Experiment. Dec 2012. URL <https://cds.cern.ch/record/1502664/>. Cited on pages 1, 17, 26, and 28.
- [2] B.H. Bransden and C.J. Joachain. *Quantum mechanics*. Pearson Education, second edition, 2000. Cited on page 3.
- [3] Sven-Patrik Hallsjö. Covering the sphere with noncontextuality inequalities. Bachelor's thesis, Linköping University, The Institute of Technology, 2013. URL [http://urn.kb.se/resolve?urn=urn:nbn:se:liu:diva-103663](http://urn.kb.se/resolve?urn=urn:nbn:se:liu.diva-103663). Cited on page 3.
- [4] A. Zee. *Quantum Field Theory in a Nutshell*. Princeton University Press, illustrated edition edition, March 2003. ISBN 0691010196. Cited on pages 3, 6, and 7.
- [5] Herbert Goldstein, Charles P. Poole, and John L. Safko. *Classical Mechanics (3rd Edition)*. Addison-Wesley, 3 edition, June 2001. ISBN 0201657023. Cited on page 3.
- [6] W. E. Burcham and M. Jobes. *Nuclear and Particle Physics*. Pearson education, second edition, 1995. Cited on page 4.
- [7] The ATLAS Collaboration. Observation of a new particle in the search for the Standard Model Higgs boson with the ATLAS detector at the LHC. *Phys. Lett. B*, 716(arXiv:1207.7214). CERN-PH-EP-2012-218):1–29. 39 p, Aug 2012. Cited on page 4.
- [8] Standard model of elementary particles. http://en.wikipedia.org/wiki/File:Standard_Model_of_Elementary_Particles.svg, 2014. Accessed: 2014-03-24. Cited on page 4.
- [9] G. Jungman, M. Kamionkowski, and K. Griest. Supersymmetric dark matter. *Physics Reports*, 267:195–373, March 1996. doi: 10.1016/0370-1573(95)00058-5. Cited on pages 4 and 5.

- 1015 [10] NASA. NASA's solar system exploration: the planets: orbits and
1016 physical characteristics. <https://solarsystem.nasa.gov/planets/>
1017 charchart.cfm, 2014. Accessed: 2014-03-21. Cited on page 6.
- 1018 [11] T. S. van Albada, J. N. Bahcall, K. Begeman, and R. Sancisi. Distribution
1019 of dark matter in the spiral galaxy NGC 3198. *Astrophysical Journal*, 295:
1020 305–313, August 1985. doi: 10.1086/163375. Cited on page 6.
- 1021 [12] Jessica Goodman, Masahiro Ibe, Arvind Rajaraman, William Shepherd,
1022 Tim M.P. Tait, et al. Constraints on Light Majorana dark Matter from Colliders.
1023 *Phys.Lett.*, B695:185–188, 2011. doi: 10.1016/j.physletb.2010.11.009.
1024 Cited on pages 5 and 7.
- 1025 [13] ATLAS Collaboration. Search for dark matter candidates and large extra di-
1026 mensions in events with a jet and missing transverse momentum with the at-
1027 las detector. *J. High Energy Phys.*, 04(arXiv:1210.4491. CERN-PH-EP-2012-
1028 210):075. 58 p, October 2012. URL [http://cds.cern.ch/record/](http://cds.cern.ch/record/1485031)
1029 1485031. Cited on pages 5, 8, and 9.
- 1030 [14] J. Goodman, M. Ibe, A. Rajaraman, W. Shepherd, T. M. P. Tait, and H.-B. Yu.
1031 Constraints on dark matter from colliders. *Phys.Rev.D82:116010,2010*, 82
1032 (11):116010, December 2010. doi: 10.1103/PhysRevD.82.116010. Cited on
1033 page 7.
- 1034 [15] ATLAS. Atlas luminosity public results. <https://twiki.cern.ch/twiki/bin/view/AtlasPublic/LuminosityPublicResults>, 2013.
1035 Accessed: 2014-03-06. Cited on page 10.
- 1036 [16] AC Team. The four main LHC experiments, Jun 1999. URL <http://cds.cern.ch/record/40525>. Cited on page 10.
- 1037 [17] Werner Herr and B Muratori. Concept of luminosity. 2006. URL <http://cds.cern.ch/record/941318/>. Cited on page 11.
- 1038 [18] The ATLAS Collaboration. The atlas experiment at the cern large hadron col-
1039 linder. *Journal of Instrumentation*, 3(08):S08003. 437 p, 2008. URL <https://cdsweb.cern.ch/record/1129811/>. Cited on pages 11 and 12.
- 1040 [19] Joao Pequenao. Computer generated image of the whole ATLAS detector,
1041 Mar 2008. URL <http://cds.cern.ch/record/1095924>. Cited on page
1042 12.
- 1043 [20] ATLAS Collaboration. Event display for one of the monojet candidates in
1044 the data. The event has a jet with $\text{pt} = 602 \text{ GeV}$ at $\eta = -1$ and $\phi =$
1045 2.6 , $\text{MET} = 523 \text{ GeV}$, and no additional jet with $\text{pt}_{\text{jet}} > 30 \text{ GeV}$ in the fi-
1046 nal state.. [https://atlas.web.cern.ch/Atlas/GROUPS/PHYSICS/](https://atlas.web.cern.ch/Atlas/GROUPS/PHYSICS/CONFNOTES/ATLAS-CONF-2011-096/fig_08.png)
1047 [CONFNOTES/ATLAS-CONF-2011-096/fig_08.png](https://atlas.web.cern.ch/Atlas/GROUPS/PHYSICS/CONFNOTES/ATLAS-CONF-2011-096/fig_08.png), 2011. Accessed:
1048 2014-03-28. Cited on page 13.
- 1049 [21] ATLAS Collaboration. Physics at a High-Luminosity LHC with ATLAS. Jul
1050

- 1054 2013. URL <https://cds.cern.ch/record/1564937>. Cited on page
1055 15.
- 1056 [22] J. Alwall, M. Herquet, F. Maltoni, O. Mattelaer, and T. Stelzer. MadGraph
1057 5: going beyond. *Journal of High Energy Physics*, 6:128, June 2011. doi:
1058 10.1007/JHEP06(2011)128. Cited on page 15.
- 1059 [23] Torbjörn Sjöstrand, Stephen Mrenna, and Peter Skands. A brief introduc-
1060 tion to {PYTHIA} 8.1. *Computer Physics Communications*, 178(11):852 –
1061 867, 2008. ISSN 0010-4655. doi: [http://dx.doi.org/10.1016/j.cpc.2008.
1062 01.036](http://dx.doi.org/10.1016/j.cpc.2008.01.036). URL [http://www.sciencedirect.com/science/article/
1063 pii/S0010465508000441](http://www.sciencedirect.com/science/article/pii/S0010465508000441). Cited on page 15.
- 1064 [24] The ROOT Team. Root. <http://root.cern.ch/drupal/>, 2014. Ac-
1065 cessed: 2014-03-28. Cited on page 15.
- 1066 [25] S. Agostinelli, J. Allison, K. Amako, J. Apostolakis, H. Araujo, P. Arce,
1067 M. Asai, D. Axen, S. Banerjee, G. Barrand, F. Behner, L. Bellagamba,
1068 J. Boudreau, L. Broglia, A. Brunengo, H. Burkhardt, S. Chauvie, J. Chuma,
1069 R. Chytracek, G. Cooperman, G. Cosmo, P. Degtyarenko, A. Dell'Acqua,
1070 G. Depaola, D. Dietrich, R. Enami, A. Feliciello, C. Ferguson, H. Fe-
1071 sefeldt, G. Folger, F. Foppiano, A. Forti, S. Garelli, S. Giani, R. Gi-
1072 annitrapani, D. Gibin, J.J. Gómez Cadenas, I. González, G. Gracia
1073 Abril, G. Greeniaus, W. Greiner, V. Grichine, A. Grossheim, S. Guatelli,
1074 P. Gumligner, R. Hamatsu, K. Hashimoto, H. Hasui, A. Heikkinen,
1075 A. Howard, V. Ivanchenko, A. Johnson, F.W. Jones, J. Kallenbach, N. Kanaya,
1076 M. Kawabata, Y. Kawabata, M. Kawaguti, S. Kelner, P. Kent, A. Kimura,
1077 T. Kodama, R. Kokoulin, M. Kossov, H. Kurashige, E. Lamanna, T. Lampén,
1078 V. Lara, V. Lefebure, F. Lei, M. Liendl, W. Lockman, F. Longo, S. Magni,
1079 M. Maire, E. Medernach, K. Minamimoto, P. Mora de Freitas, Y. Morita,
1080 K. Murakami, M. Nagamatu, R. Nartallo, P. Nieminen, T. Nishimura, K. Oht-
1081 subo, M. Okamura, S. O'Neale, Y. Oohata, K. Paech, J. Perl, A. Pfeiffer,
1082 M.G. Pia, F. Ranjard, A. Rybin, S. Sadilov, E. Di Salvo, G. Santin, T. Sasaki,
1083 N. Savvas, Y. Sawada, S. Scherer, S. Sei, V. Sirotenko, D. Smith, N. Starkov,
1084 H. Stoecker, J. Sulkimo, M. Takahata, S. Tanaka, E. Tcherniaev, E. Safai
1085 Tehrani, M. Tropeano, P. Truscott, H. Uno, L. Urban, P. Urban, M. Verderi,
1086 A. Walkden, W. Wander, H. Weber, J.P. Wellisch, T. Wenaus, D.C. Williams,
1087 D. Wright, T. Yamada, H. Yoshida, and D. Zschiesche. Geant4—a sim-
1088 ulation toolkit. *Nuclear Instruments and Methods in Physics Research
1089 Section A: Accelerators, Spectrometers, Detectors and Associated Equipment*,
1090 506(3):250 – 303, 2003. ISSN 0168-9002. doi: [http://dx.doi.org/
1091 10.1016/S0168-9002\(03\)01368-8](http://dx.doi.org/10.1016/S0168-9002(03)01368-8). URL <http://www.sciencedirect.com/science/article/pii/S0168900203013688>. Cited on page 17.
- 1092 [26] ATLAS Collaboration. Performance assumptions for an upgraded ATLAS
1093 detector at a High-Luminosity LHC. Mar 2013. URL [https://cds.cern.
1094 ch/record/1527529/](https://cds.cern.ch/record/1527529/). Cited on pages 17, 20, 26, 27, and 28.
- 1095 [27] ATLAS Collaboration. Electron performance measurements with the ATLAS

1097 detector using the 2010 LHC proton-proton collision data. *Eur. Phys. J. C*,
1098 72(arXiv:1110.3174. CERN-PH-EP-2011-117):1909. 45 p, Oct 2011. Com-
1099 ments: 33 pages plus author list (45 pages total), 24 figures, 12 tables, sub-
1100 mitted to Eur. Phys. J. C. Cited on pages 26 and 28.

1101 [28] ATLAS Collaboration. Search for New Phenomena in Monojet plus Missing
1102 Transverse Momentum Final States using 10fb-1 of pp Collisions at $\sqrt{s}=8$
1103 TeV with the ATLAS detector at the LHC. Nov 2012. URL <http://cds.cern.ch/record/1493486/>. Cited on pages 32, 34, 35, and 37.

1105 [29] Donald Duck. The history of automatic control. *Duckburg Journal of Sci-
1106 ence*, 106(3):345–401, 2005. Cited on page 46.

1108 **Upphovsrätt**

1109 Detta dokument hålls tillgängligt på Internet — eller dess framtida ersättare —
 1110 under 25 år från publiceringsdatum under förutsättning att inga extraordinära
 1111 omständigheter uppstår.

1112 Tillgång till dokumentet innebär tillstånd för var och en att läsa, ladda ner,
 1113 skriva ut enstaka kopior för enskilt bruk och att använda det oförändrat för icke-
 1114 kommersiell forskning och för undervisning. Överföring av upphovsrätten vid
 1115 en senare tidpunkt kan inte upphäva detta tillstånd. All annan användning av
 1116 dokumentet kräver upphovsmannens medgivande. För att garantera äktheten,
 1117 säkerheten och tillgängligheten finns det lösningar av teknisk och administrativ
 1118 art.

1119 Upphovsmannens ideella rätt innehåller rätt att bli nämnd som upphovsman
 1120 i den omfattning som god sed kräver vid användning av dokumentet på ovan
 1121 beskrivna sätt samt skydd mot att dokumentet ändras eller presenteras i sådan
 1122 form eller i sådant sammanhang som är kränkande för upphovsmannens litterära
 1123 eller konstnärliga anseende eller egenart.

1124 För ytterligare information om Linköping University Electronic Press se för-
 1125 lagets hemsida <http://www.ep.liu.se/>

1126 **Copyright**

1127 The publishers will keep this document online on the Internet — or its possi-
 1128 ble replacement — for a period of 25 years from the date of publication barring
 1129 exceptional circumstances.

1130 The online availability of the document implies a permanent permission for
 1131 anyone to read, to download, to print out single copies for his/her own use and
 1132 to use it unchanged for any non-commercial research and educational purpose.
 1133 Subsequent transfers of copyright cannot revoke this permission. All other uses
 1134 of the document are conditional on the consent of the copyright owner. The
 1135 publisher has taken technical and administrative measures to assure authenticity,
 1136 security and accessibility.

1137 According to intellectual property law the author has the right to be men-
 1138 tioned when his/her work is accessed as described above and to be protected
 1139 against infringement.

1140 For additional information about the Linköping University Electronic Press
 1141 and its procedures for publication and for assurance of document integrity, please
 1142 refer to its www home page: <http://www.ep.liu.se/>